Journal Pre-proofs

Phytotoxicity of silver nanoparticles on *Vicia faba*: evaluation of particle size effects on photosynthetic performance and leaf gas exchange

William F. Falco, Marisa D. Scherer, Samuel L. Oliveira, Heberton Wender, Ian Colbeck, Tracy Lawson, Anderson R.L. Caires

PII: S0048-9697(19)34807-7
DOI: https://doi.org/10.1016/j.scitotenv.2019.134816
Reference: STOTEN 134816

To appear in: *Science of the Total Environment*

Received Date: 12 September 2019
Revised Date: 29 September 2019
Accepted Date: 3 October 2019

Please cite this article as: W.F. Falco, M.D. Scherer, S.L. Oliveira, H. Wender, I. Colbeck, T. Lawson, A.R.L. Caires, Phytotoxicity of silver nanoparticles on *Vicia faba*: evaluation of particle size effects on photosynthetic performance and leaf gas exchange, *Science of the Total Environment* (2019), doi: https://doi.org/10.1016/j.scitotenv.2019.134816

Phytotoxicity of silver nanoparticles on *Vicia faba*: evaluation of particle size effects on photosynthetic performance and leaf gas exchange

William F. Falco[a], Marisa D. Scherer[b], Samuel L. Oliveira[b], Heberton Wender[b], Ian Colbeck[c], Tracy Lawson[c], Anderson R. L. Caires[b,c,*]

[a] Grupo de Óptica Aplicada, Universidade Federal da Grande Dourados, CP 533, 79804-970 Dourados, MS, Brazil.

[b] Grupo de Óptica e Fotônica, Instituto de Física, Universidade Federal de Mato Grosso do Sul, CP 549, 790070-900 Campo Grande, MS, Brazil.

[c] School of Life Sciences, University of Essex, Colchester CO4 3SQ, UK.

.

Abstract

Nanotechnology is an emerging field in science and engineering, which presents significant impacts on the economy, society and the environment. The nanomaterials' (NMs) production, use, and disposal is inevitably leading to their release into the environment where there are uncertainties about its fate, behaviour, and toxicity. Recent works have demonstrated that NMs can penetrate, translocate, and accumulate in plants. However, studies about the effects of the NMs on plants are still limited because most investigations are carried out in the initial stage of plant development. The present study aimed to evaluate and characterize the photochemical efficiency of photosystem II (PSII) of broad bean (*Vicia faba*) leaves when subjected to silver nanoparticles (AgNPs) with

diameters of 20, 51, and 73 nm as well as to micrometer-size Ag particles (AgBulk). The AgNPs were characterized by transmission electron microscopy and dynamic light scattering. The analyses were performed by injecting the leaves with 100 mg L^{-1} aqueous solution of Ag and measuring the chlorophyll fluorescence imaging, gas exchange, thermal imaging, and reactive oxygen species (ROS) production. In addition, silver ion (Ag^{+}) release from Ag particles was determined by dialysis. The results revealed that AgNPs induce a decrease in the photochemical efficiency of photosystem II (PSII) and an increase in the non-photochemical quenching. The data also revealed that AgNPs affected the stomatal conductance (g_s) and CO_2 assimilation. Further, AgNPs induced an overproduction of ROS in *Vicia faba* leaves. Finally, all observed effects were particle diameter-dependent, increasing with the reduction of AgNPs diameter and revealing that AgBulk caused only a small or no changes on plants. In summary, the results point out that AgNPs may negatively affect the photosynthesis process when accumulated in the leaves, and that the NPs themselves were mainly responsible since negligible Ag^{+} release was detected.

Keywords: *Vicia faba*, Photosynthetic performance, Silver nanoparticle, Nanoparticle diameter effect, Toxicity.

* Corresponding author. E-mail address: anderson.caires@ufms.br

1. Introduction

The use of nanomaterials (NMs) in commercial products has raised concerns about the impacts on the environment and human health as its commercialization preceded a regulatory framework dealing with their use, storage, and disposal (Lai et al., 2018). NMs behave differently to their respective bulk materials with macro- or microscopic

dimensions (Hulla et al., 2015). For example, when in nanometric dimensions, the available effective area of the material is increased so that the interactions with molecules changes (Bouwmeester et al., 2009; Dhar et al., 2015). Besides, materials in the nanometric scale show distinct effects of conductivity, reactivity and optical sensitivity as compared to ones in the bulk material (Nel et al., 2015). Based on that, NMs can generate adverse biological effects on living cells. Recent studies have proved the toxicity of nanoparticles (NPs) such as fullerene, carbon nanotubes, metal, and metal oxides in human cells, bacteria, and rodents (Sun et al., 2013; Yang et al., 2013). For instance, silver nanoparticles (AgNPs) induce adverse effects on ammonia oxidizing bacteria, compromising its nitrification ability (Beddow et al., 2014). They also can cause structural chromosomal aberrations in so far as the AgNPs reach the cell nucleus (Patlolla et al., 2012). It is estimated that more than 20 tons of AgNPs are produced annually only in the United States whereas global production is around 300 tons per year (Starnes et al., 2015). Antibacterial properties are one of the most appreciated characteristics of AgNPs, so they are widely used in the manufacture of pharmaceuticals and personal care products (Starnes et al. 2015).

In this scenario, the understanding of the interactions between NPs and plants is fundamental because plants are the basis of food chains and essential in all ecosystems. However the NPs impact on plants depends on their composition, concentration, size, and physicochemical properties as well as on the plant species. NPs can penetrate living plant tissues and migrate to different regions of the plant. They may also be absorbed by plant roots and transported to the aerial part through the vascular system (Feichtmeier et al., 2015). Studies have shown that NPs can inhibit plant growth and germination (Pradhan et al., 2015; Singh and Kumar, 2015). Additionally, NPs can be also transferred through the food chain causing a trophic magnification (Judy et al., 2011).

Despite the research already reported involving the interaction between NPs and plants, most of the studies have investigated the NPs effects at an early stage of plant development so that questions remain unanswered such the role of NP size (i.e., the role of the total surface area) as a phytotoxic parameter affecting the photosynthetic activity of higher plants. It is very important to understand how NP size alters the photosynthesis process such as evaluating the possible changes on CO_2 assimilation rate, and photosystem II (PSII) efficiency for example.

Chlorophyll fluorescence has been used as a precise and non-destructive technique for studying the photosynthetic efficiency, which provides an indicator of perturbation in plant metabolism and a good indicator of stress (Baker 2008).

Higher plants are sensitive to the harmful potential of pollutants in which *Vicia faba, Allium cepa, Tradescantia, Zea mays, Nicotiana tabacum, Hordeum vulgare,* and *Crepis capillaris* are among the most used plant species as bioindicators (Leme and Marin-Morales, 2009). Here, *Vicia faba* plants were chosen for investigating the physiological changes induced by AgNPs with different diameters and bulk silver (AgBulk) at a later stage of plant growth. Thus, the present study reports the toxicity dependence of AgBulk (micrometer-size particles) and AgNPs with three different diameters (20, 51, and 73 nm) when internalized in *Vicia faba* leaves using a well-established toxic nanoparticle concentration of 100 mg L^{-1} (Kumari et al., 2009; Scherer et al., 2019).

2. Materials and Methods

2.1 Silver nanoparticles

PVP-coated AgNPs in aqueous solution (*nanoComposix*) with nominal diameters of 25, 50, and 75 nm were used. Silver microparticles (AgBulk) with

diameters in the 5-8 μm range were also employed (*Sigma Aldrich*). The AgBulk aqueous solution was prepared by dispersing the powder in distilled water using ultrasonic agitation for 30 min. The concentration of the AgNPs and AgBulk was set at 100 mg L^{-1} in all experiments.

2.2 AgNPs Characterization

The characterization of the AgNPs was performed by transmission electron microscopy (TEM) with energy dispersive spectroscopy (EDS) using an FEI Tecnai G2 microscope operating at 200 kV. AgNPs solutions were shaken by ultrasound during 10 min to ensure the particles are dispersed and well mixed. A drop of this solution was deposited on a carbon film using a copper grid for microscopy and dried for 24 h before measurements. Analyses of morphology and particles diameter distribution were carried out using ImageJ software.

The aqueous solutions containing the AgNPs with different diameters were also evaluated by dynamic light scattering (DLS) to obtain the hydrodynamic radius distribution and the polydispersity index (*PDI*). The DLS was performed in a Malvern ZetaSizer Nano ZS90 with a laser at 633 nm. The scattered light was monitored at 90 and 173°. The measurements were performed in a glass cuvette with four polished faces and 10-mm optical path. The AgNPs in aqueous solution were diluted in deionized water (3 mg L^{-1}) for these measurements (Bhattacharjee, 2016; Dorranian et al., 2013; Kass et al., 2017).

The study of the Ag^{+} ions released from the AgNPs in distilled water was performed, based on Besinis et al. 2014 (Besinis et al., 2014) with modifications. The experiments used dialysis tubing (Sigma-Aldrich) with molecular weight cut-off at 12,000 Da (with an approximate exclusion diameter of 2.5 nm). 3 mL of AgNPs at 100

mg L^{-1} filled the dialysis tubing; then, it was placed in a beaker containing 247 mL of distilled water, totaling 250 mL. The silver concentration in the filtrate solution was determined by collecting 25 mL of water from the beaker after 96 h and determining the Ag content in a Thermo iCAP 6300 Duo ICP OES (Thermo Fisher Scientific). The Ag^{+} concentration was determined considering the Ag content before ultrafiltration.

2.3 Broad Bean Plants

The *Vicia faba* seeds were sown in plastic pots containing a commercial substrate for horticulture and kept in a greenhouse with temperatures of 22/18 ºC day/night, humidity of 65/70% day/night, and a photoperiod of 12/12 h day/night with a luminous intensity of about 300 µmol.m^{-2}.s^{-1} (Karuppanapandian et al., 2017). Experiments were performed on a minimum of 5 and a maximum of 10 plants per treatment conditional to the technique, providing a suitable statistic in the case of image analyses (Baker, 2008; Murchie and Lawson, 2013).

In vivo analyses started 20 days after planting when the leaves to be analysed were completely expanded. The measurements were taken at zero time right before the solution injection (BI) in the second pair of leaves. All analyses were performed on the same leaves. The plants received the solution injection in the left leaf. The right leaf was kept as control, receiving the only an injection of distilled water, free of metallic particles. About 1.5 mL of solution was injected at the beginning of the central vein of each leaf. The solution was shaken in an ultrasonic bath for 5 min prior to injection into the plant. The measurements were performed daily (every 24 h) over a week until 168 h after the injection. It is worth pointing out that the nanoparticle injection process was chosen from others (pulverization, irrigation, etc), despite it being a non-natural way of how

nanoparticles would enter leaves, because we aimed to investigate the direct relationship between photosynthetic efficiency and nanoparticle concentration inside leaves.

2.4 Chlorophyll *a* Fluorescence Imaging

Experiments to examine the influence of the AgNPs on the photosynthetic apparatus of *in vivo* plants were done in a *Technologica CFImager*, containing 1600 blue LEDs (470 nm), saturation pulse capacity of up to 6000 µmol m^{-2} s^{-1} and maximum continuous light intensity of 2000 µmol m^{-2} s^{-1}. A progressive scanning CCD camera (AVT Stingray SXGA + 2/3") was used to acquire the fluorescence images with a resolution of 696 x 519 pixels. This system is closed so that external brightness doesn't affect the plant. Before the measurements, the plants were adapted to the dark for 30 min to ensure the opening of all reaction centers in the leaves. An optical filter selected the chlorophyll emission with a peak at 680 nm. The measurements were performed on the youngest fully expanded leaves. The protocol used to obtain the fluorescence kinetics was based on incident light intensity of 600 µmol m^{-2} s^{-1} and a long time (until 20 min) for light adaptation (Baker, 2008; Murchie and Lawson, 2013).

2.5 Gas exchange analysis

CO_2 assimilation rate (*A*) analysis was assessed as a function of the internal CO_2 concentration (*Ci*) known as an *A/Ci* curve using an Infra-red gas analyser (CIRAS–1 system (*PP Systems*, USA). An incident light intensity of 1060 µmol m^{-2} s^{-1} was used and the CO_2 varied from 50 to 1800 µmol m^{-2} s^{-1}. All *A/Ci* curves were measured and analysed at 25 ^{o}C and the maximum carboxylation of Rubisco (*Vc,max*) and regeneration of RuBP (*Jmax*) rates were determined from the *A/Ci* curve following the methods of (Bernacchi

et al., 2001; Mcmurtrie and Wang, 1992). *A/Ci* curves were collected from five plants for each treatment at 72 h after the solution injection. The equipment analysed a leaf area of 2.5 cm^2 (1.78 cm diameter).

Measurements of the stomatal conductance (g_s) versus time were performed before injection and every 24 h after injection during a week until 168 h. The CO_2 was set at 400 μmol m^{-2} s^{-1} and the light intensity at 300 μmol m^{-2} s^{-1}. These values are similar to those in which the plants were maintained during germination and growth. The plants were adapted to the environmental lighting 1 h prior analyses. All gas exchange measures were performed on the abaxial leaf surface as it has a higher stomatal density.

2.6 Thermography

Thermal images were recorded with an infrared thermal camera (E6 FLIR Systems) which had lenses with a field of view of 45º x 34º, resolution of 320 x 240 pixels, thermal sensitivity < 0.06 ºC, and maximum frequency of 9 Hz. The FLIR Tools software was used in the analysis of the thermal images.

2.7 Microscopic Analysis of Leaves

The microscopic studies of the broad bean leaves were made in an *Olympus - BX60*. The stomatal density was determined with a 10x lens. The images were collected by a CCD camera (*Olympus*) with the resolution of 2592 x 1944 pixels and handled using the *TSView 7.1* software.

Leaf impressions were taken on the abaxial leaf surfaces using polysiloxane based Xantopren Heraeus (WEYERS and JOHANSEN, 1985). Immediately prior, Xantopren was mixed with the universal activator for mold curing. Then, the mixture was applied to the abaxial leaf surface and left to dry for about 1 min. The mold was removed from the

leaves with the assistance of tweezers. After removal, a quick-drying and transparent nail polish was deposited on the mold. The film was removed and placed on a glass slide for the microscopic analysis. As this is a non-destructive approach, it was possible to study the leaves for one week. Impression were obtained and the stomatal density was analysed at zero time (BI), 24, 96, and 168 h after the solution injection into the leaves.

2.8 Reactive Oxygen Species Analysis

The study of the reactive oxygen species in broad bean leaves was done using the fluorescent marker 2',7' *Dichlorofluorescin diacetate* (H2DCF-DA) (*Sigma Aldrich*). H2DCF-DA is a probe capable of permeabilizing cells, being cleaved by intracellular esterases generating the anion ($H2DCF^-$), which presents low fluorescent in its reduced stated, and then the $H2DCF^-$ may be oxized by the ROS forming a highly fluorescent molecule (DCF) in its oxidized state (Chen et al., 2010; Wen et al., 2016). Consequently, H2DCF-DA acts as an intracellular ROS indicator. Before introduction in the leaves, a H2DCF-DA stock solution was prepared with HPLC-grade ethanol (5 mM). The stock solution was diluted to 1 mM in 10 mM TRIS-HCl buffer. Later, the AgNPs and AgBulk diluted in distilled water were added to the solution (Baccelli et al., 2014; Grunberg and Taleisnik, 2015; Kyselakova et al., 2013; Zabala et al., 2015).

Broad bean leaves were treated with the H2DCF-DA solution by transpiration (Driever et al., 2009). The leaves were detached from the stem with a blade. This procedure was done with the stem submerged in water to avoid air bubbles that may interfere in the internalization procedure of the H2DCF-DA solution. Next, the solution was assimilated by the leaves by transpiration immersing only the petiole (stem connecting the leaf to the stalk) in the DCF solution for 2.5 h under red light (~ 650 nm) with the intensity of 50 μmol m^{-2} s^{-1}. The red light was used to avoid the H2DCF-DA

degradation that absorbs radiation in the 430-530 nm interval (Gomes et al., 2005). The leaves were removed from the H2DCF-DA solution and again subjected to red light with an intensity of 100 μmol m^{-2} s^{-1} for 30 min. Following, a CCD camera and an emission filter at 525 nm collected the ROS marker emission images from leaves. An LED was used as the excitation source operating at 470 nm. The excitation was applied on the leaves by a pulse lasting nearly 3 s to avoid the ROS marker degradation (Driever et al., 2009).

3 Results

3.1 AgNPs Characterization

Table 1 summarizes the characteristics of the AgNPs obtained from the TEM and DLS measurements. For nominal diameters ($D_{nominal}$) of 25, 50, and 75 nm, equivalent mean diameters (D_{TEM}) of 20 ± 7, 51 ± 7, and 73 ± 5 nm were measured by TEM, respectively. The transmission electron micrographs, particle diameter distributions, and EDS spectra of the AgNPs are presented in Fig. 1. The nanoparticles with spherical shapes were uniformly distributed. EDS measurements confirmed silver as the chemical composition of the NPs. The observed Cu lines were originated from the copper grid used as a support during the microscopy analysis. Further, SEM analysis showed that AgBulk is composed by micrometric particles with irregular shape and sizes in the 0.8–3.0 μm range (Fig. S1 in the supplementary materials).

The AgNPs with the diameter of 20 and 51 nm released 0.30 and 0.04% of Ag^+ regarding the Ag total, respectively (Table 1). An Ag^+ concentration below of the limit of quantification (LOQ) was detected for the 73-nm AgNPs. Therefore, the Ag^+ liberation in distilled water was diameter-dependent as a result of the larger total surface areas of

the smaller AgNPs (Wang et al., 2014). These data are in accordance with previous studies that observed that the AgNPs-PVP are stable in aqueous solution, releasing less than 1% of Ag^+ species (Cvjetko et al., 2017; Nallanthighal et al., 2017; Scherer et al., 2019). PVP strongly binds to the nanoparticles surface avoiding aggregation (Nallanthighal et al., 2017).

Higher hydrodynamic diameters ($D_{hydrodynamic}$) were measured when compared with the respective ones determined by TEM (D_{TEM}) (Table 1). In fact, $D_{hydrodynamic}$ is usually higher than D_{TEM} because DLS assess the total diameter provided by the AgNPs along with ions and molecules (layers) adsorbed on the surface nanoparticles (Bhattacharjee, 2016; Dorranian et al., 2013; Kass et al., 2017)(Bhattacharjee, 2016)(Bhattacharjee, 2016)(Bhattacharjee, 2016) . The AgNPs are monodisperse in the aqueous medium since the polydispersity index (PDI) is in the 0.06–0.17. A sample is defined highly monodisperse when the PDI $\leq$ 0.1, nearly monodisperse for values between 0.1 and 0.7, and highly polydisperse for values > 0.7 (Stetefeld et al., 2016). Besides, although PVP as a neutral polymer should lead to a net surface charge close to zero in the AgNPs-PVP, the zeta potential data revealed that the nanoparticle surfaces were negatively charged for ions or structures attached to them after synthesis (Cvjetko et al., 2017; Michalke and Vinković-Vrček, 2018).

3.2 Plant bioassays

Chlorophyll fluorescence imaging was used for investigating the effects of the AgNPs on plant metabolism of mature leaves. The maximum quantum efficiency (*Fv*/*Fm*), operating efficiency of PSII (*Fq'*/*Fm'*), and non-photochemical quenching (NPQ) were determined. Figure 2 shows representative images of *Fv*/*Fm* in which distilled water was injected in the left leaf (control), while an aqueous solution containing

20-nm AgNPs at 100 mg L^{-1} was injected in the right leaf. BI is the leaf image collected before injection. The application of AgNPs induced a significant reduction in *Fv*/*Fm* values after 24 h in the whole leaf. However, *Fv*/*Fm* recovered to the originally values after 168 h, and similar values to the ones related to the control leaf.

Figure 3 indicates that the *Fv*/*Fm* alteration was AgNPs diameter-dependent. *Fv*/*Fm* was reduced to a greater extent by decreasing the nanoparticle diameter. Furthermore AgBulk produced no significant change in *Fv*/*Fm*. Figure 4 presents the percentage variation of *Fv*/*Fm* regarding the control leaf for different times.

The quantum efficiency of PSII under light-adapted conditions (*Fq'*/*Fm*'), was affected by both the AgBulk and AgNPs (Fig. 5). The decrease in the *Fq'*/*Fm*' values were greatest with the application of the smallest particles. In addition, the 20-nm AgNPs induced a more rapid reduction in *Fq'*/*Fm*', while a gradual reduction was observed for the 51-nm and 73-nm AgNPs and AgBulk.

The chlorophyll imaging showed that values of NPQ show increased in the leaves containing the AgNPs (Fig. 6). So, NPs caused an increase in the dissipation of light energy by non-photochemical ways rather than photochemical processes. The AgNPs with diameters of 20 and 51 nm induced a change in the NPQ after 24h.

It is worth noting that, at the end of the measurements, small spots of necrosis on the leaf surface could be noticed by visual inspection for the leaves submitted to the AgNPs, which the leaf damage was AgNPs diameter-dependent. However, necrosis occurred more pronounced on the abaxial side of the leaf as can be seen in Fig. 7, while almost no visible damage can be seen on the adaxial side of the leaf.

Gas exchange analysis was also carried out to better characterize the AgNPs effects on the photosynthetic activity of the leaves, evaluating the alterations on the CO_2

assimilation rate caused by AgNPs. Fig. 8 shows the *A*/*Ci* curve where it can be observed that the CO_2 assimilation rate (*A*) is drastically reduced due to the AgNPs into the leaves. The data show that AgNPs of 20 nm promoted the highest reduction while leaves submitted to the AgBulk behaved similarly to the control leaves. Although the AgNPs of 51 nm and 73 nm also altered the CO_2 assimilation, both nanoparticles induced similar *A* reduction.

Following Bernacchi et al., (2001) and Mcmurtrie and Wang (1992), the maximum carboxylation rate of Rubisco (Vc_{max}) (Figure 9 (a)) and the maximum electron transport rate (J_{max}) [i.e., the maximum regeneration rate of the RuBP] (Figure 9 (b)) were determined. Vc_{max} was reduced in the presence of both AgNPs and AgBulk, indicating that carbon fixation was reduced by the Ag-containing solutions. However, a diameter-dependent behavior was observed, in which AgNPs reduction was statistically higher than AgBulk. The J_{max} values also significantly decreased in the presence of AgNPs, whereas the AgBulk did not induce a statistically significant reduction in relation to the control.

The CO_2 assimilation rate (*A*) was also monitored as a function of time as presented in Fig. 10. The results show a drastic reduction of *A* 24 h after the AgNPs injection, especially for 20 nm where a decrease of 73% was detected. However, the *A* value remained almost constant for all AgNPs injected leaves after the initial reduction during the first 48 h. However, a small decrease was induced by AgBulk, but the CO_2 assimilation rate recovered to values similar to those of the control leaves after 120 h.

Stomatal conductance (g_s) results (Fig. 11) revealed that Ag-containing solution reduced g_s and the reduction was higher for smaller particles. As previously observed for the other parameters, the AgNPs of 20 nm induced the greatest effect. However, g_s in the

leaves containing AgBulk, which initially reduced after the injection, was recovered after 120 h.

Aiming to eliminate any hypothesis of a relation between the changes in the gas exchange and stomatal density, optical microscopy measurements were performed and the stomatal density of the leaves submitted to the AgNPs was determined. The shows that the stomatal density values were not statistically different among all analyzed leaves (i.e., leaves submitted to the AgNPs of 20, 51 and 73 nm as well as AgBulk), which a value in the 35 to 45 stomata/mm^2 range was obtained (Fig. S2 in the supplementary materials). In fact, this behavior was already expected, since the injection of the Ag particles in the leaves was carried out when they were already fully expanded.

Thermal images of the leaves were collected and the leaf temperature was determined and monitored as a function of the time. The results revealed that both AgBulk and AgNPs did not significantly alter the leaf surface temperature (Fig. S3 in the supplementary materials), except for the AgNPs of 20 nm which induced an increase in the temperature after 144 h of the injection process. A representative image of the temperature elevation observed in the leaf with AgNPs of 20 nm after 168 h is shown in the Fig. S4 in the supplementary.

The ROS production stimulated by the presence of the silver particles in the leaves was measured. Fig. 12 shows the representative images of the DCF (a fluorescent marker generated by the ROS formation in the leaves) as a function of the Ag particle size. The data revealed an increase in ROS generation due to Ag particles where the ROS production was higher for smaller particles. All Ag-containing solutions induced statistically significant increases in ROS production compared to control leaves, which a quantitative analysis of ROS marker emission promoted by the presence of Ag is

presented in Fig. 13. These results demonstrated that the ROS production increased with the decrease of the particle diameter. A percentage rise of 17 ± 3, 33 ± 3, 40 ± 5, 101 ± 19 % of the ROS production was promoted by the AgBulk, AgNPs of 51, 73, and 20 nm, respectively. It is important to stress that the control leaves received only a fluorescent marker and water.

4 Discussion

In brief, the results demonstrated that silver particles, especially in nanometric dimensions, may be toxic when internalized and accumulated in *Vicia faba* leaves, impairing photosynthesis and, in some cases, causing the death of leaf tissue due to the production and accumulation of ROS in the leaves. Additionally, the data also showed that the particle diameter was an important factor of toxicity as all studied parameters were particle-size dependent, which the highest effects induced by the smallest particles. It is worth pointing out that the AgBulk induced small phytotoxic effects but, in most cases, the leaves were able to recover.

The AgNPs put the plants under stress conditions, decreasing the CO_2 assimilation rate and altering the functioning of photosystem II (PSII). Meanwhile, NPQ values increased significantly, revealing that Ag particles induced an increase in the energy dissipation in PSII, an expected photoprotective response in the chloroplast for plants under stress conditions (Demmig-Adams and Adams, 1992). It is well established that, under stress conditions, a reduction of the rate of linear electron transport as well as a decrease in the accumulation of H+ in thylakoid lumen may be induced by the reduction of CO_2 assimilation, which limits the demand for NADPH and ATP. In this condition, the NPQ and the downregulation of linear electron flow at cytochrome b6/f can be significantly increased as a photoprotective response in the chloroplast, protecting the electron transport chain against over-reduction (Joliot and Johnson, 2011).

Our data indicated that the observed effects were probably highly correlated with the presence of intracellular reactive oxygen species (ROS). Although ROS can be generated by AgNPs or Ag ions, the present findings indicated that the ROS are mainly produced by the interaction of O_2 with the AgNPs surface since negligible silver dissolution was determined (see Table 1). (Nallanthighal et al., 2017). As recently demonstrated in a paper published by our research group, Ag ions play as a minor contributor to the toxicity of the PVP-coated AgNPs when released at concentrations lower than 1% (Scherer et al., 2019). Consequently, a minimal contribution of Ag^+ toxicity is expected. Furthermore, Qian et al (2013) recently demonstrated that AgNPs can induce more intense oxidative stress than Ag ions (Qian et al., 2013). By analyzing the effects of AgNPs and Ag ions on the expression of antioxidant enzymes in *A. thaliana*, it was observed that the expression of various antioxidant enzyme genes increased upon exposure to the low concentration of AgNPs while Ag ions did not significantly change the transcription of antioxidant enzymes (Qian et al., 2013).

A review of the literature confirms that AgNPs may induce an overproduction of ROS, which damages the structures of chloroplasts, lipids, and DNA macromolecules (Karami Mehrian and De Lima, 2016; Qian et al., 2013; RASTOGI et al., 2019; Syu et al., 2014). In addition, the ROS overproduction triggered by the AgNPs may also damage chloroplasts, inhibit plant growth, and reduce plant cellular viability (Karami,Reza, and Fatemeh 2015; Oukarroum et al. 2013; Qian et al. 2013; Sosan et al. 2016).

The observed changes in the physiological status of the *Vicia faba* may be the result of a series of factors. For instance, a reduction in the number of thylakoids or photosynthetic pigments can result in a decrease in the photosynthetic yield (Kirchho et al., 2000; Vinit-dunand et al., 2002). It was demonstrated that AgNPs induced a decrease of the total chlorophyll content in *A. thaliana* seedlings after 2 weeks of exposure (Abdel-

Azeem and Elsayed, 2014; Qian et al., 2013). This study also reported that, after treatment with AgNPs, the chloroplasts were slightly flatter, the grana lamellae became thinner and ambiguous, and the distance between the thylakoid membranes became wider (Abdel-Azeem and Elsayed, 2014; Qian et al., 2013). In fact, the AgNPs can inhibit the chlorophyll biosynthesis, which will reduce the photosynthetic efficiency and provoke an imbalance in the water content in the leaves (Abdel-Azeem and Elsayed, 2014; Qian et al., 2013). Consequently, it is expected a reduction in the rate of stomatal conductance, resulting in a lower rate of gas exchange and a consequent reduction in CO_2 assimilation (Soil et al., 2012; Sosan et al., 2016). In addition, it may not be ruled out that direct effects of AgNPs on stomatal conductance can reduce the CO_2 assimilation, decreasing the photosynthetic efficiency. Furthermore, a reduction in the photosynthetic activity will usually be related to an increase in the NPQ, since a portion of the absorbed light energy which should be used to drive photosynthesis is dissipated as heat.

It is well known that oxygen-dependent metabolic processes, such as aerobic respiration (which occurs in mitochondria), photosynthesis (in chloroplasts) and photorespiration (in peroxisomes) lead to the production of ROS. However, singlet oxygen ($^1O_2$), for example, is generated almost entirely in PSII, in chloroplasts (Resende et al., 2003). As the lifetime of $^1O_2$ is very small, its active sites are probably close to where they are produced (Rehman et al., 2013; Resende et al., 2003). Thus the effects induced by $^1O_2$ initiate mainly inside the chloroplasts (i.e., close to PSII). Differently, the other ROS species, such as $O_2^{\bullet-}$, H_2O_2, and $OH^{\bullet}$, are generated in chloroplasts, mitochondria, and peroxisomes. However, the literature suggests that the greatest amount of these ROS is generated by the electron transport chain (ETC) in both chloroplasts and mitochondria. For example, the formation of H_2O_2 via ETC is about 4 mol m^{-2} s^{-1} while only 10 µmol m^{-2} s^{-1} is produced in the peroxisomes, in the photorespiration pathway

(Barbosa et al., 2014; Foyer and Shigeoka, 2011). Nevertheless, it is important to point out that the literature also indicates that the mitochondria are the main ROS generators in heterotrophic cells, being a minor contributor to the total ROS production in photosynthetic cells (Barbosa et al., 2014; Queval et al., 2008). Therefore, considering that the majority of ROS generated in plants under stress conditions comes from chloroplasts, our results indicated that AgNPs have effectively acted in this chloroplasts as AgNPs induced the production and accumulation of ROS in the leaves.

It is important to note that the AgNPs caused a reduction of the PSII efficiency. However, the observed reduction was not so strong, as *Fv/Fm* does not reach a value lower than 0.6, decreasing just about 12% in relation to the control leaves for the smallest diameter tested. The observed *Fv/Fm* Fv/F decrease may be attributed to ETC deactivation, which entails a sequence of events, leading to the reduction to the ATP and NADPH production in the light phase of photosynthesis, compromising the operation of the Calvin cycle and reducing the carbon fixation, and, consequently, producing a lower content of glycosides and starch. In addition, previous studies carried out by our research group studies demonstrated that metal nanoparticles can suppress the Chl emission by transferring the excited electron of Chl to the metal surface (Falco et al., 2015, 2011; Queiroz et al., 2016). Thus, the NPs may be inhibiting the electron transport chain, inducing an increase in the energy dissipation by non-photochemical pathways and consequently reducing the photochemical activities of the plants (Barazzouk et al., 2005; Falco et al., 2011; Vinit-dunand et al., 2002). In spite of contributing, this effect is possibly not the decisive event for the cellular death observed in the necrotic parts of the leaves. Most likely, the main cause for cell death (necrosis) was the ROS production and accumulation as ROS are able to kill cells by oxidizing them.

The ETC deactivation by AgNPs changes the electron flow between PSII and PSI,

may also induce the energy transfer from excited Chl to the O_2 molecules, promoting molecular oxygen in the ground state ($^3O_2$ – triplet state) to the excited state ($^1O_2$ – singlet state) $^1O_2$, a very reactive ROS. Then, the singlet oxygen may cause degradation in protein D1, at a rate higher than the antioxidative defense responses of the plant (Keren et al., 1997; Kojima et al., 2007). Protein D1 is part of the structural construction of PSII and its degradation due to oxidative stress leads to irreversible degradation of thylakoids, followed by chloroplasts and consequent cell death (Aroz et al., 1994; Lupínková et al., 2004). This is the same route of action used by herbicides, which act as deactivators of ETC in chloroplasts, inhibiting photosynthesis and degrading D1 protein due to the oxidative stress induced by the accumulation of $^1O_2$ (Altha and Orlani, 2007; Fuerst and Norman, 2013; Qian et al., 2013). However, other species of ROS may be formed due to the presence of AgNPs in fava leaves and may be contributing concomitantly to oxidative stress. The AgNPs that have become negatively electrified by the ETC deactivation can provide electrons for the creation of ROS radicals, which can be formed by the successive transfer of electrons from AgNPs to O_2, combined with the protons available in the chloroplasts. Thus, besides the generation of singlet oxygen, the AgNPs may be favouring the accentuated generation of superoxide radicals, hydrogen peroxide as well as hydroxyl radicals. This phenomenon may have occurred in the mitochondria simultaneously, but less intense. For instance, the AgNPs can act as a toxic agent in the mitochondria due to the ROS production (Hsin et al., 2008) because the ROS may damage cell membrane, disrupt the ATP production pathway and DNA replication, and change gene expression (Moreno-Garrido et al., 2015).

Several studies have reported an increase in the activities of antioxidant enzymes as well as non-enzymatic antioxidants in plants submitted to metals, suggesting the involvement of the antioxidative defense system of plants in response to the stress caused

by several metallic particles (Felici et al., 2014; Kumar et al., 2014; Sharma et al., 2016; Srivastava and Pandey, 2014). However, the action of the antioxidative defense system of plants, in response to the oxidative stress induced by the NPs, may be not enough to promote a tolerance to the accumulation of the NPs in the plants (Sharma et al., 2012), especially depending on the size of AgNPs as demonstrated in the present study. Additionally, although NPs internalized into the cells play a major contribution to the phytotoxic effects in the leaves, the side effects induced by the AgNPs located among the cells should not be ruled out. For instance, AgNPs may limit the nutrients` mobility, acting as physical barriers, blocking the vessels and veins, which transport water and nutrients from the soil to the leaves, as well as blocking the stomata and, consequently, affecting the leaf gas exchange.

In summary, the present study provides further information on the phytotoxic and cytotoxic of AgNPs in *Vicia faba* leaves, demonstrating an increment in toxicity with decreasing NPs diameter likely due to their internalization in the tissues. This effect may be related to the fact that small NPs can reach regions where larger particles are not able to reach. Addtionally smaller NPs provide a much larger total surface area that enables a more effective interaction with the plant cells, generating increased ROS and enhancing damage of the cells (Feizi et al., 2013; Wang et al., 2015). Recent studies have observed that the cellular interaction with the AgNPs and ROS generation are higher as smaller is the NPs diameter (Carlson et al., 2008; Scherer et al., 2019). The small particle diameter and larger total surface area may permit NPs to move through the cell wall pores and reach the plasma membrane (Samberg et al., 2011). In fact, the uptake, translocation, and accumulation of AgNPs in cells depends on the particle size and plant cell structure and permeability (Carlson et al., 2008; Li et al., 2015).

3.2 Conclusion

The present study demonstrated that AgNPs induced alterations on the photochemical efficiency of PSII, stomatal conductance (g_s), and CO_2 assimilation rate of *Vicia faba* leaves. The effects were diameter-dependent because they increased with a reduction of the AgNPs diameter as well as small or no change were induced by AgBulk. These effects are a result of the higher total surface area of the smaller nanoparticles, being more toxic and reactive for the cells at a fixed concentration. The data revealed that AgNPs caused a decrease in the stomatal conductance (g_s), CO_2 assimilation, and photosynthetic activity of the leaves as well as an increase in the non-photochemical quenching (NPQ), possibly due to the overproduction of ROS induced by AgNPs as a negligible Ag^+ release was caused by the NPs. In addition, the results also suggest that the electrons of the excited chlorophylls could be transferred to the metal surface of the NPs, deactivating the electron transport chain, which implies the reduction of photosynthetic yield associated with an oxidative stress, increasing the ROS generation. The results also demonstrated that AgNPs caused small spots of necrosis on the leaf surface as a result of the oxidative damage caused by the ROS overproduction. In summary, the results demonstrated that AgNPs might negatively affect the photosynthesis activity when internalized and accumulated in the leaves, revealing that AgNPs were responsible for the side effects since negligible Ag^+ release was detected.

Conflicts of interest

There are no conflicts to declare.

Acknowledgements

This study was financed in part by the Coordenação de Aperfeiçoamento de Pessoal de Nível Superior - Brasil (CAPES) - Finance Code 001. The authors acknowledge the financial support provided by the CAPES-PrInt funding program (grant numbers: 88887.353061/2019-00 and 88887.311920/2018-00) and the National Institute of Science and Technology of Basic Optics and Optics Applied to Life Science (grant number: 465360/2014-9). The authors are grateful to CNPq, CAPES and FUNDECT, Brazilian funding agencies, for their financial support. The authors also would like to acknowledge G. Machado, and V.A. Nascimento for the nanoparticle characterization support.

References

Abdel-Azeem, E., Elsayed, B., 2014. Phytotoxicity of silver nanoparticles on Vicia faba seedlings.

Altha, C.É.R.A.M., Orlani, G.I.F., 2007. Synthesis of 3- (4-Bromobenzyl) -5- (aryl methylene) -5 H -furan-2-ones and Their Activity as Inhibitors of the Photosynthetic Electron Transport Chain 8562–8569.

Aroz, E., Mccaffery, S., Anderson, J.M., 1994. Recovery from Photoinhibition in Peas (Pisum sativum 1 .) Acclimated to Varying Growth Irradiances ’ 1033–1041.

Baccelli, I., Lombardi, L., Luti, S., Bernardi, R., Picciarelli, P., Scala, A., Pazzagli, L., 2014. Cerato-Platanin Induces Resistance in Arabidopsis Leaves through Stomatal Perception , Overexpression of Salicylic Acid- and Ethylene-Signalling Genes and Camalexin Biosynthesis 9, 1–11. https://doi.org/10.1371/journal.pone.0100959

Baker, N.R., 2008. Chlorophyll Fluorescence: A Probe of Photosynthesis In Vivo. Annu. Rev. Plant Biol. 59, 89–113. https://doi.org/10.1146/annurev.arplant.59.032607.092759

Barazzouk, S., Kamat, P. V., Hotchandani, S., 2005. Photoinduced Electron Transfer between Chlorophyll a and Gold Nanoparticles. J. Phys. Chem. B 109, 716–723. https://doi.org/10.1021/jp046474s

Barbosa, M.R., Willadino, L., Ulisses, C., Camara, T.R., 2014. Geração e desintoxicação enzimática de espécies reativas de oxigênio em plantas 453–460.

Beddow, J., Stolpe, B., Cole, P., Lead, J.R., Sapp, M., Lyons, B.P., Colbeck, I., Whitby, C., 2014. Effects of engineered silver nanoparticles on the growth and activity of ecologically important microbes 6, 448–458. https://doi.org/10.1111/1758-2229.12147

Bernacchi, C.J., Singsaas, E.L., Pimentel, C., Jr, A.R.P., Long, S.P., 2001. Improved temperature response functions for models of Rubisco-limited photosynthesis 253–259.

Besinis, A., De Peralta, T., Handy, R.D., 2014. The antibacterial effects of silver, titanium dioxide and silica dioxide nanoparticles compared to the dental disinfectant chlorhexidine on Streptococcus mutans using a suite of bioassays. Nanotoxicology 8, 1–16. https://doi.org/10.3109/17435390.2012.742935

Bhattacharjee, S., 2016. DLS and zeta potential - What they are and what they are not? J. Control. Release 235, 337–351. https://doi.org/10.1016/j.jconrel.2016.06.017

Bouwmeester, H., Dekkers, S., Noordam, M.Y., Hagens, W.I., Bulder, A.S., Heer, C. De, Sandra, E.C.G., Wijnhoven, S.W.P., Marvin, H.J.P., Sips, A.J.A.M., 2009. Review of health safety aspects of nanotechnologies in food production. Regul. Toxicol. Pharmacol. 53, 52–62. https://doi.org/10.1016/j.yrtph.2008.10.008

Carlson, C., Hussein, S.M., Schrand, A.M., Braydich-Stolle, L.K., Hess, K.L., Jones, R.L., Schlager, J.J., 2008. Unique cellular interaction of silver nanoparticles: Size-dependent generation of reactive oxygen species. J. Phys. Chem. B 112, 13608–13619. https://doi.org/10.1021/jp712087m

Chen, X., Zhong, Z., Xu, Z., Chen, L., Wang, Y., 2010. 2′,7′-Dichlorodihydrofluorescein as a fluorescent probe for reactive oxygen species measurement: Forty years of application and controversy. Free Radic. Res. 44, 587–604. https://doi.org/10.3109/10715761003709802

Cvjetko, P., Milošić, A., Domijan, A.M., Vinković Vrček, I., Tolić, S., Peharec Štefanić, P., Letofsky-Papst, I., Tkalec, M., Balen, B., 2017. Toxicity of silver ions and differently coated silver nanoparticles in Allium cepa roots. Ecotoxicol. Environ. Saf. 137, 18–28. https://doi.org/10.1016/j.ecoenv.2016.11.009

Demmig-Adams, B., Adams, W.W., 1992. Photoprotection and Other Responses of Plants to High Light Stress. Annu. Rev. Plant Physiol. Plant Mol. Biol. 43, 599–626. https://doi.org/10.1146/annurev.pp.43.060192.003123

Dhar, A., Prabha, S., Sillanpää, M., Kwon, Y., Lee, C., Varma, R.S., 2015. Fate of engineered nanoparticles : Implications in the environment. Coord. Chem. Rev. 287, 64–78. https://doi.org/10.1016/j.ccr.2014.12.014

Dorranian, D., Tajmir, S., Khazanehfar, F., 2013. Effect of Laser Fluence on the Characteristics of Ag Nanoparticles Produced by Laser Ablation 2013, 93–100.

Driever, S., MJ, F., PM, M., NR, B., 2009. T. Pfannschmidt (Ed.),. https://doi.org/10.1007/978-1-59745-289-2

Falco, W.F., Botero, E.R., Falcão, E.A., Santiago, E.F., Bagnato, V.S., Caires, A.R.L., 2011. In vivo observation of chlorophyll fluorescence quenching induced by gold nanoparticles. J. Photochem. Photobiol. A Chem. 225, 65–71. https://doi.org/10.1016/j.jphotochem.2011.09.027

Falco, W.F., Queiroz, A.M., Fernandes, J., Botero, E.R., Falcão, E.A., Guimarães, F.E.G., Peko, J.M., Oliveira, S.L., Colbeck, I., Caires, A.R.L., 2015. Journal of Photochemistry and Photobiology A : Chemistry Interaction between chlorophyll and silver nanoparticles : A close analysis of chlorophyll fl uorescence quenching 299, 203–209.

Feichtmeier, N.S., Walther, P., Leopold, K., 2015. Uptake , effects , and regeneration of barley plants exposed to gold nanoparticles. https://doi.org/10.1007/s11356-014-4015-0

Feizi, H., Kamali, M., Jafari, L., Rezvani Moghaddam, P., 2013. Phytotoxicity and stimulatory impacts of nanosized and bulk titanium dioxide on fennel (Foeniculum vulgare Mill). Chemosphere 91, 506–511. https://doi.org/10.1016/j.chemosphere.2012.12.012

Felici, E., Molina, A., Almeida, C., Baldo, M.F., Zirulnik, F., Gomez, M.R., 2014. C

admium-induced mechanisms in G lycine oxidative damage and antioxidant defense 2, 791–798. https://doi.org/10.12980/JCLM.2.2014JCLM-2014-0077

Foyer, C.H., Shigeoka, S., 2011. Understanding Oxidative Stress and Antioxidant Functions to Enhance Photosynthesis 1 155, 93–100. https://doi.org/10.1104/pp.110.166181

Fuerst, E.P., Norman, M.A., 2013. Weed Science Society of America Interactions of Herbicides with Photosynthetic Electron Transport Interactions of Herbicides with Photosynthetic Electron Transport1 39, 458–464.

Gomes, A., Fernandes, E., Lima, J.L.F.C., 2005. Fluorescence probes used for detection of reactive oxygen species. J. Biochem. Biophys. Methods 65, 45–80. https://doi.org/10.1016/j.jbbm.2005.10.003

Grunberg, K.A., Taleisnik, E.L., 2015. Reactive Oxygen Species in the Elongation Zone of Maize Leaves Are Necessary for Leaf Extension 1. https://doi.org/10.1104/pp.001222.activity

Hsin, Y.H., Chen, C.F., Huang, S., Shih, T.S., Lai, P.S., Chueh, P.J., 2008. The apoptotic effect of nanosilver is mediated by a ROS- and JNK-dependent mechanism involving the mitochondrial pathway in NIH3T3 cells. Toxicol. Lett. 179, 130–139. https://doi.org/10.1016/j.toxlet.2008.04.015

Hulla, J.E., Sahu, S.C., Hayes, A.W., 2015. Nanotechnology : History and future 34, 1318–1321. https://doi.org/10.1177/0960327115603588

Joliot, P., Johnson, G.N., 2011. Regulation of cyclic and linear electron flow in higher plants. Proc. Natl. Acad. Sci. 108, 13317–13322. https://doi.org/10.1073/pnas.1110189108

Judy, J.D., Unrine, J.M., Bertsch, P.M., 2011. Evidence for biomagnification of gold nanoparticles within a terrestrial food chain. Environ. Sci. Technol. 45, 776–781. https://doi.org/10.1021/es103031a

Karami Mehrian, S., De Lima, R., 2016. Nanoparticles cyto and genotoxicity in plants: Mechanisms and abnormalities. Environ. Nanotechnology, Monit. Manag. 6, 184–193. https://doi.org/10.1016/j.enmm.2016.08.003

Karami, S., Reza, M., Fatemeh, H., 2015. Effect of silver nanoparticles on free amino acids content and antioxidant defense system of tomato plants. Indian J. Plant Physiol. https://doi.org/10.1007/s40502-015-0171-6

Karuppanapandian, T., Geilfus, C., Mühling, K., Novák, O., Gloser, V., 2017. Plant Science Early changes of the pH of the apoplast are different in leaves , stem and roots of Vicia faba L . under declining water availability. Plant Sci. 255, 51–58. https://doi.org/10.1016/j.plantsci.2016.11.010

Kass, M. El, Brohan, L., Gautier, N., Ø, B., David, C.Ø., 2017. TiO 2 Anatase Solutions for Electron Transporting Layers in Organic Photovoltaic Cells 2390–2396. https://doi.org/10.1002/cphc.201700306

Keren, N., BERG, A., KAN, P.J.M. VAN, LEVANON, H., OHAD, I., 1997. Mechanism of photosystem II photoinactivation and D1 protein degradation at low

light : The role of back electron flow 94, 1579–1584.

Kirchho, H., Horstmann, S., Weis, E., 2000. Control of the photosynthetic electron transport by PQ di ¡ usion microdomains in thylakoids of higher plants 1459, 148–168.

Kojima, K., Oshita, M., Nanjo, Y., Kasai, K., Tozawa, Y., Hayashi, H., Nishiyama, Y., 2007. Oxidation of elongation factor G inhibits the synthesis of the D1 protein of photosystem II 65, 936–947. https://doi.org/10.1111/j.1365-2958.2007.05836.x

Kumar, A., Pratap, R., Pradyumna, S., Singh, K., Selenium, Á.R.Á., 2014. Selenium ameliorates arsenic induced oxidative stress through modulation of antioxidant enzymes and thiols in rice (Oryza sativa L .) 1153–1163. https://doi.org/10.1007/s10646-014-1257-z

Kumari, M., Mukherjee, A., Chandrasekaran, N., 2009. Genotoxicity of silver nanoparticles in Allium cepa. Sci. Total Environ. 407, 5243–5246. https://doi.org/10.1016/j.scitotenv.2009.06.024

Kyselakova et al., 2013. Reactive Oxygen and Nitrogen Species and Hormone Signalling in Systemic Infection of Pea by Pea enation mosaic virus 49, 105–119.

Lai, R.W.S., Yeung, K.Y., Yung, M.M.N., Djurišić B., A., Giesy, J.P., Leung, K.M.Y., 2018. Regulation of engineered nanomaterials : current challenges , insights and future directions 3060–3077. https://doi.org/10.1007/s11356-017-9489-0

Leme, D.M., Marin-Morales, M.A., 2009. Allium cepa test in environmental

monitoring: A review on its application. Mutat. Res. - Rev. Mutat. Res. 682, 71–81. https://doi.org/10.1016/j.mrrev.2009.06.002

Li, X., Schirmer, K., Bernard, L., Sigg, L., Pillai, S., Behra, R., 2015. Silver nanoparticle toxicity and association with the alga Euglena gracilis. Environ. Sci. Nano 2, 594–602. https://doi.org/10.1039/c5en00093a

Lupínková, L., Komenda, J., Photochemistry, S., Komenda, J., Lupı, L., 2004. Oxidative Modifications of the Photosystem II D1 Protein by Reactive Oxygen Species : From Isolated Protein to Cyanobacterial Cells Oxidative Modifications of the Photosystem II D1 Protein by Reactive Oxygen Species : From Isolated Protein to Cyanobacteri 79, 152–162.

Mcmurtrie, R., Wang, Y., 1992. Mathematical models of the photosynthetic response of tree stands to rising CO2 concentrations and temperatures.

Michalke, B., Vinković-Vrček, I., 2018. Speciation of nano and ionic form of silver with capillary electrophoresis-inductively coupled plasma mass spectrometry. J. Chromatogr. A 1572, 162–171. https://doi.org/10.1016/j.chroma.2018.08.031

Moreno-Garrido, I., Pérez, S., Blasco, J., 2015. Toxicity of silver and gold nanoparticles on marine microalgae. Mar. Environ. Res. 111, 60–73. https://doi.org/10.1016/j.marenvres.2015.05.008

Murchie, E.H., Lawson, T., 2013. Chlorophyll fluorescence analysis : a guide to good practice and understanding some new applications 64, 3983–3998. https://doi.org/10.1093/jxb/ert208

Nallanthighal, S., Chan, C., Bharali, D.J., Mousa, S.A., Vásquez, E., Reliene, R., 2017. Particle coatings but not silver ions mediate genotoxicity of ingested silver nanoparticles in a mouse model. NanoImpact 5, 92–100. https://doi.org/10.1016/j.impact.2017.01.003

Nel, A., Xia, T., Madler, L., Li, N., 2015. Toxic Potential of Materials at the Nanolevel 622–628.

Oukarroum, A., BARHOUMI, L., PIRASTRU, L., DEWEZ, D., 2013. SILVER NANOPARTICLE TOXICITY EFFECT ON GROWTH AND CELLULAR VIABILITY OF THE AQUATIC PLANT LEMNA GIBBA 32, 902–907. https://doi.org/10.1002/etc.2131

Patlolla, A.K., Berry, A., May, L., Tchounwou, P.B., 2012. Genotoxicity of silver nanoparticles in Vicia faba: A pilot study on the environmental monitoring of nanoparticles. Int. J. Environ. Res. Public Health 9, 1649–1662. https://doi.org/10.3390/ijerph9051649

Pradhan, S., Patra, P., Mitra, S., Dey, K.K., Basu, S., Chandra, S., Palit, P., Goswami, A., 2015. Copper nanoparticle (CuNP) nanochain arrays with a reduced toxicity response: A biophysical and biochemical outlook on Vigna radiata. J. Agric. Food Chem. 63, 2606–2617. https://doi.org/10.1021/jf504614w

Qian, H., Peng, X., Han, X., Ren, J., Sun, L., Fu, Z., 2013. Comparison of the toxicity of silver nanoparticles and silver ions on the growth of terrestrial plant model Arabidopsis thaliana. J. Environ. Sci. 25, 1947–1956. https://doi.org/10.1016/S1001-0742(12)60301-5

Queiroz, A.M., Mezacasa, A.V., Graciano, D.E., Falco, W.F., M'Peko, J.-C., Guimarães, F.E.G., Lawson, T., Colbeck, I., Oliveira, S.L., Caires, A.R.L., 2016. Quenching of chlorophyll fluorescence induced by silver nanoparticles. Spectrochim. Acta - Part A Mol. Biomol. Spectrosc. 168. https://doi.org/10.1016/j.saa.2016.05.033

Queval, G., Hager, J., Gakiere, B., Noctor, G., 2008. Why are literature data for H 2 O 2 contents so variable ? A discussion of potential difficulties in the quantitative assay of leaf extracts 59, 135–146. https://doi.org/10.1093/jxb/erm193

RASTOGI, A., ZIVCAK, M., TRIPATHI, D.K., YADAV, S., KALAJI, H.M., 2019. Phytotoxic effect of silver nanoparticles in Triticum aestivum: Improper regulation of photosystem I activity as the reason for oxidative damage in the chloroplast. Photosynthetica 57, 209–216. https://doi.org/10.32615/ps.2019.019

Rehman, A.U., Cser, K., Sass, L., Vass, I., 2013. Characterization of singlet oxygen production and its involvement in photodamage of Photosystem II in the cyanobacterium Synechocystis PCC 6803 by histidine-mediated chemical trapping. Biochim. Biophys. Acta - Bioenerg. 1827, 689–698. https://doi.org/10.1016/j.bbabio.2013.02.016

Resende, M.L. V, Salgado, S.M.L., Chaves, Z.M., 2003. Espécies Ativas de Oxigênio na Resposta de Defesa de Plantas a Patógenos 123–130.

Samberg, M.E., Orndorff, P.E., Monteiro-Riviere, N.A., 2011. Antibacterial efficacy of silver nanoparticles of different sizes, surface conditions and synthesis methods. Nanotoxicology 5, 244–253. https://doi.org/10.3109/17435390.2010.525669

Scherer, M.D., Sposito, J.C.V., Falco, W.F., Grisolia, A.B., Andrade, L.H.C., Lima, S.M., Machado, G., Nascimento, V.A., Gonçalves, D.A., Wender, H., Oliveira, S.L., Caires, A.R.L., 2019. Cytotoxic and genotoxic effects of silver nanoparticles on meristematic cells of Allium cepa roots: A close analysis of particle size dependence. Sci. Total Environ. 660, 459–467. https://doi.org/10.1016/j.scitotenv.2018.12.444

Sharma, P., Jha, A.B., Dubey, R.S., Pessarakli, M., 2012. Reactive Oxygen Species , Oxidative Damage , and Antioxidative Defense Mechanism in Plants under Stressful Conditions 2012. https://doi.org/10.1155/2012/217037

Sharma, P., Kumar, A., Bhardwaj, R., 2016. Plant steroidal hormone epibrassinolide regulate – Heavy metal stress tolerance in Oryza sativa L . by modulating antioxidant defense expression. Environ. Exp. Bot. 122, 1–9. https://doi.org/10.1016/j.envexpbot.2015.08.005

Singh, D., Kumar, A., 2015. Effects of Nano Silver Oxide and Silver Ions on Growth of Vigna radiata Effects of Nano Silver Oxide and Silver Ions on Growth of Vigna radiata. Bull. Environ. Contam. Toxicol. 95, 379–384. https://doi.org/10.1007/s00128-015-1595-4

Soil, B., Solymosi, K., Bertrand, M., 2012. Soil metals , chloroplasts , and secure crop production : a review To cite this version : HAL Id : hal-00930487 Soil metals , chloroplasts , and secure crop production : a review. https://doi.org/10.1007/s13593-011-0019-z

Sosan, A., Svistunenko, D., Straltsova, D., Tsiurkina, K., Smolich, I., Lawson, T.,

Subramaniam, S., Golovko, V., Anderson, D., Sokolik, A., Colbeck, I., Demidchik, V., 2016. Engineered silver nanoparticles are sensed at the plasma membrane and dramatically modify the physiology of Arabidopsis thaliana plants 245–257. https://doi.org/10.1111/tpj.13105

Srivastava, R.K., Pandey, P., 2014. Cadmium and lead interactive effects on oxidative stress and antioxidative responses in rice seedlings. https://doi.org/10.1007/s00709-014-0614-3

Starnes, D.L., Unrine, J.M., Starnes, C.P., Collin, B.E., Oostveen, K., Ma, R., Lowry, G. V, Bertsch, P.M., Olga, V., 2015. Impact of sulfidation on the bioavailability and toxicity of silver nanoparticles to Caenorhabditis elegans 0–25.

Stetefeld, J., McKenna, S.A., Patel, T.R., 2016. Dynamic light scattering: a practical guide and applications in biomedical sciences. Biophys. Rev. 8, 409–427. https://doi.org/10.1007/s12551-016-0218-6

Sun, J., Zhang, Q., Wang, Z., Yan, B., 2013. Effects of nanotoxicity on female reproductivity and fetal development in animal models. Int. J. Mol. Sci. 14, 9319–9337. https://doi.org/10.3390/ijms14059319

Syu, Y. yu, Hung, J.H., Chen, J.C., Chuang, H. wen, 2014. Impacts of size and shape of silver nanoparticles on Arabidopsis plant growth and gene expression. Plant Physiol. Biochem. 83, 57–64. https://doi.org/10.1016/j.plaphy.2014.07.010

Vinit-dunand, F., Epron, D., Alaoui-sosse, B., Badot, P., 2002. Effects of copper on growth and on photosynthesis of mature and expanding leaves in cucumber plants

163, 53–58.

Wang, S., Liu, H., Zhang, Y., Xin, H., 2015. The effect of CuO NPS on reactive oxygen species and cell cycle gene expression in roots of rice. Environ. Toxicol. Chem. 34, 554–561. https://doi.org/10.1002/etc.2826

Wang, X., Ji, Z., Chang, C.H., Zhang, H., Wang, M., Liao, Y.-P., Lin, S., Meng, H., Li, R., Sun, B., Winkle, L. Van, Pinkerton, K.E., Zink, J.I., Xia, T., Nel, A.E., 2014. Use of Coated Silver Nanoparticles to Understand the Relationship of Particle Dissolution and Bioavailability to Cell and Lung Toxicological Potential. Small 10, 385–398. https://doi.org/10.1002/smll.201301597

Wen, Y., Zhang, L., Chen, Z., Sheng, X., Qiu, J., Xu, D., 2016. Co-exposure of silver nanoparticles and chiral herbicide imazethapyr to Arabidopsis thaliana: Enantioselective effects. Chemosphere 145, 207–214. https://doi.org/10.1016/j.chemosphere.2015.11.035

WEYERS, J.D.B., JOHANSEN, L.G., 1985. ACCURATE ESTIMATION OF STOMATAL APERTURE FROM SILICONE RUBBER IMPRESSIONS. New Phytol. 101, 109–115. https://doi.org/10.1111/j.1469-8137.1985.tb02820.x

Yang, Y., Wang, J., Xiu, Z., Alvarez, P.J.J., 2013. IMPACTS OF SILVER NANOPARTICLES ON CELLULAR AND TRANSCRIPTIONAL ACTIVITY OF NITROGEN-CYCLING BACTERIA 32, 1488–1494. https://doi.org/10.1002/etc.2230

Zabala, M.D.T., Littlejohn, G., Jayaraman, S., Studholme, D., Bailey, T., Lawson, T.,

Tillich, M., Licht, D., Bölter, B., Del, L., Truman, W., Mans, J., Smirnoff, N., Grant, M., 2015. and are targeted by pathogen effectors 1. https://doi.org/10.1038/nplants.2015.74

Figure and Table Captions

Table 1. Nominal diameter of nanoparticles provided by the manufacturer ($D_{nominal}$), diameter determined by transmission electron micrographs (D_{TEM}), hydrodynamic diameter ($D_{hydrodynamic}$), polydispersity index (PDI), zeta potential of the AgNPs in aqueous solution, and Ag^+ liberation (in % of the initial mass) from PVP-coated AgNPs in distilled water. Limit of quantification (LOQ).

Fig. 1. Transmission electron micrographs; B) Particle diameter distribution; C) EDS Spectra for the AgNPs. The Cu lines are due to the copper grids used in the microscopy measurements of the nanoparticles.

Fig. 2. Representative chlorophyll fluorescence images of *Fv/Fm* ratio as a function of time after injection of solution. The right leaf is the control (water injection), while the left leaf received a solution with 20-nm AgNPs at 100 mg L^{-1}.

Fig. 3. Fv/Fm as a function of time for leaves injected with water (control) and injected with: (A) AgBulk, (B) 73-nm AgNPs, (C) 51-nm AgNPs, and (F) 20-nm AgNPs. 100 mg L^{-1} was used in all Ag-containing solution. Data represent the mean ± standard error. *Statistically significant difference (t test, $p < 0.05$, $n = 5$).

Fig. 4. Fv/Fm reduction with respect to the control leaf for different times. Data represent the mean ± standard error.

Fig. 5. *Fq'/Fm'* as a function of time for leaves injected with water (control) and injected with: (A) AgBulk, (B) 73-nm AgNPs, (C) 51-nm AgNPs, and (D) 20-nm AgNPs. 100 mg L^{-1} was used in all Ag-containing solution. Data represent the mean ± standard error. *Statistically significant difference (t-test, $p < 0.05$, $n = 5$).

Fig. 6. NPQ as a function of time for leaves injected with water (control) and injected with: (A) AgBulk, (B) 73-nm AgNPs, (C) 51-nm AgNPs, and (D) 20-nm AgNPs. 100 mg L^{-1} was used in all Ag-containing solution. Data represent the mean ± standard error. *Statistically significant difference (t-test, $p < 0.05$, $n = 5$).

Fig. 7. Adaxial (upper) and abaxial (bottom) leaf surfaces. Right leaf is the control leaf (water injection) while left leaf represents the leaf injected by a solution of AgNPs of 20 nm at 100 mg L^{-1}.

Fig. 8. CO_2 assimilation rate (*A*) as a function of the internal CO_2 concentration (*Ci*) determined 72 h after the injection of the Ag-containing solutions at 100 mg L^{-1} in the leaves. Data represent the mean ± standard error.

Fig. 9. Vc, max (a) and Jmax (b) measured in the leaves injected with Ag-containing solutions at 100 mg L^{-1}. Data represent the mean ± standard error. * Significant difference (t-test, $p < 0.05$, $n = 5$).

Fig. 10. CO_2 assimilation rate (*A*) as a function of the time in the leaves submitted to: (!) H_2O, (Λ) AgBulk, (B) AgNPs 73 nm, (7) AgNPs 51 nm, and (β) AgNPs 73 nm. A concentration of 100 mg L^{-1} was used for all Ag-containing solution. Data represent the mean ± standard error.

Fig. 11. g_s as a function of time for leaves injected with water (control) and: (A) AgBulk, (B) 73 nm AgNPs, (C) 51 nm AgNPs, and (D) 20 nm AgNPs. A concentration of 100 mg L^{-1} was used for all Ag-containing solution. Data represent the mean ± standard error. *Statistically significant difference (t-test, $p < 0.05$, $n = 5$).

Fig. 12. Representative fluorescence images of the ROS marker as a function of the Ag particle diameter. The images were collected 3 h after the leaves to be exposed to the Ag-

containing solution at 100 mg L^{-1} with H2DCF-DA at 1mM. The control leaf was exposed to the H2DCF-DA and water.

Fig. 13. Fluorescence intensity of the ROS marker as a function of the diameter of the Ag particles. The emission intensities are the average intensity obtained from six leaves images collected for each treatment. Data represent the mean ± standard error. * Significant difference in relation to the control sample (t-test, $p < 0.05$, $n = 6$).

Table 1. W.F. Falco et al

$D_{nominal}$ (nm)	D_{TEM} (nm)	$D_{hydrodynamic}$ (nm)	PDI	Z (mV)	Ag^{+} (%)
25	20±7	76 ± 27	0.14	-11	0.30
50	51±7	84 ± 32	0.17	-16	0.04
75	73±5	116 ± 34	0.06	-13	< LOQ

Highlights

Phytotoxicity of AgNPs on plants of *Vicia faba* were tested

Vicia faba leaves were exposed to different AgNPs dimensions (20, 51, and 73 nm)

AgNPs were able to affect the photosynthetic activity of plants

AgNPs caused alterations on PSII activity, stomatal conductance, and CO_2 assimilation

Phytotoxic effects increased with decreasing AgNPs diameter

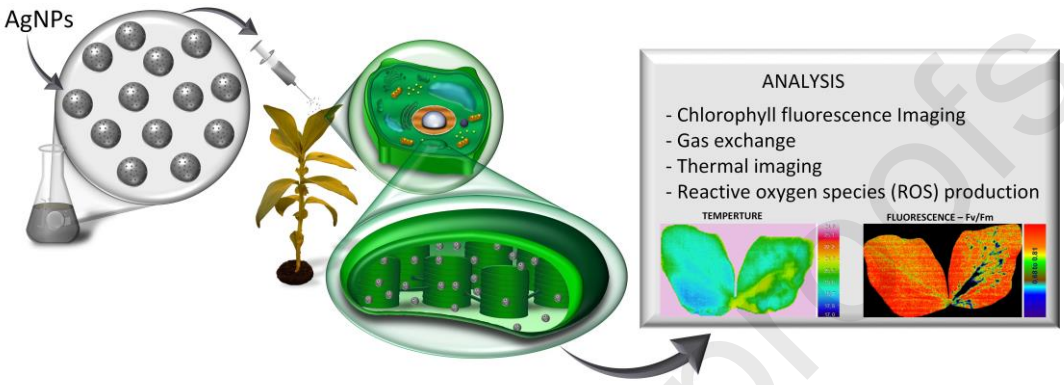

To Professor Daqiang Yin, Tongji University, Shanghai

Dear Editor

The authors declare that there is no conflict of interest.

Sincerely,

Anderson R. L. Caires

Associate Professor

Optics and Photonics Group

Institute of Physics

Federal University of Mato Grosso do Sul

E-mail: anderson.caires@ufms.br

Figure 1

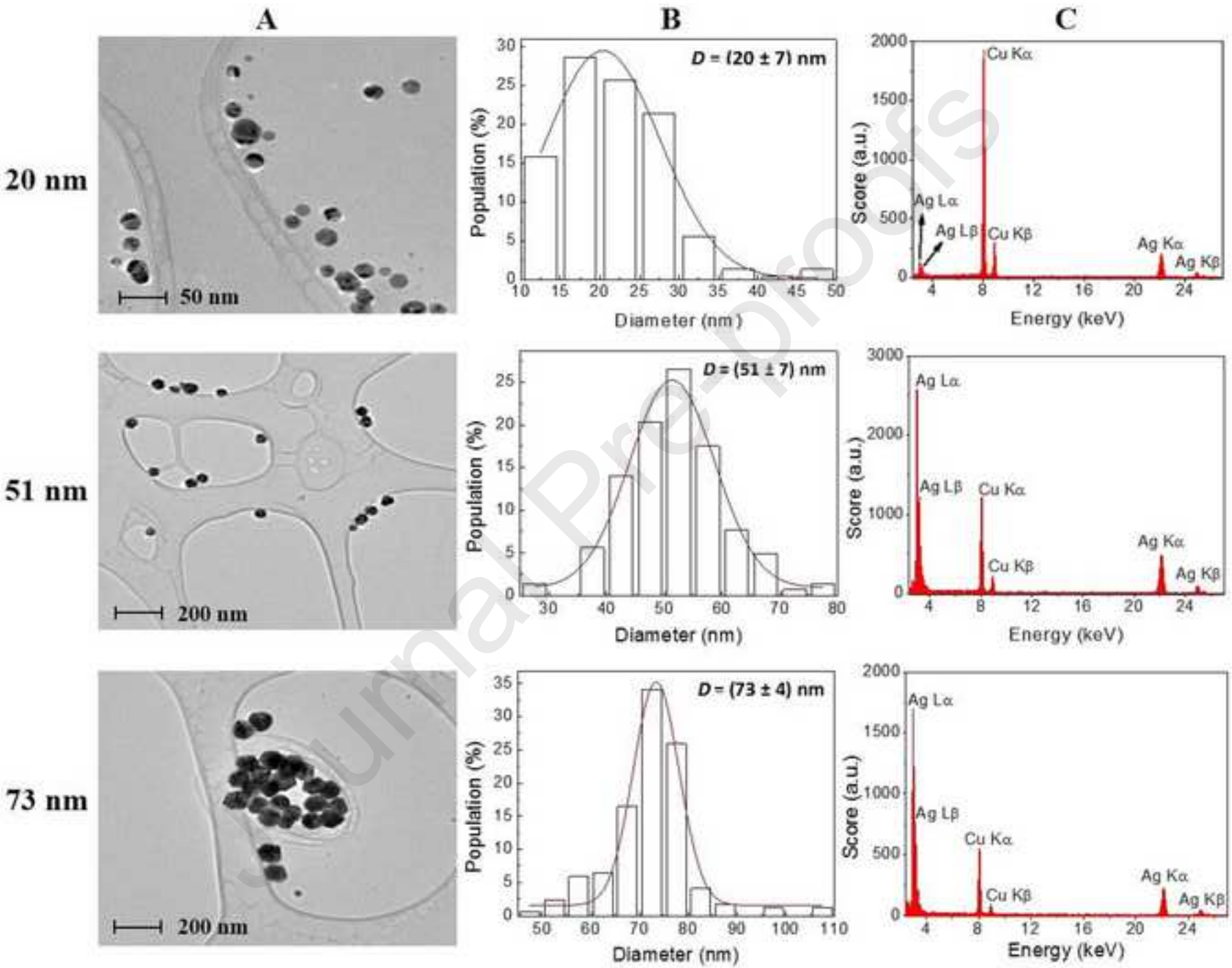

Figure 2

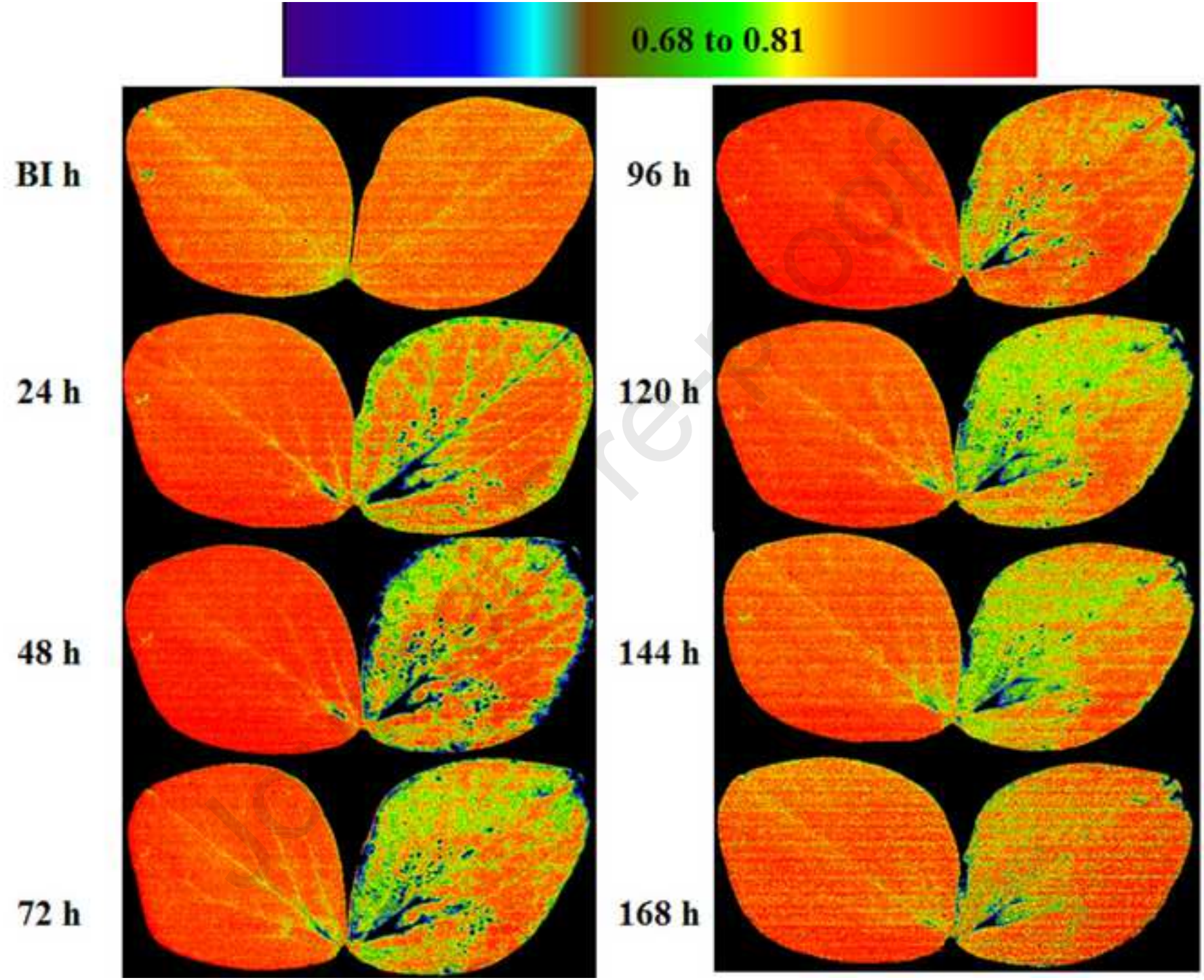

Figure 3

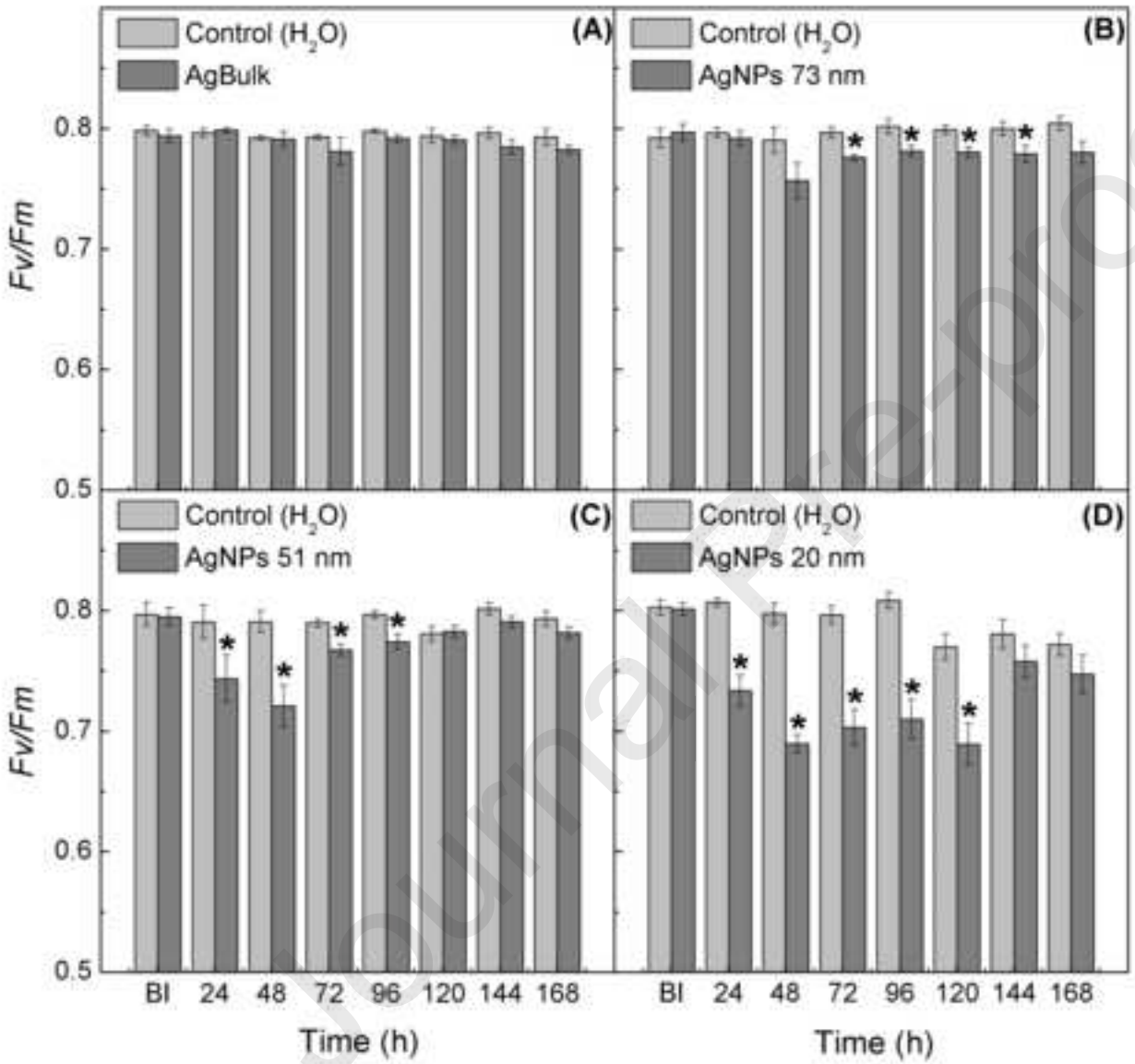

Figure 4

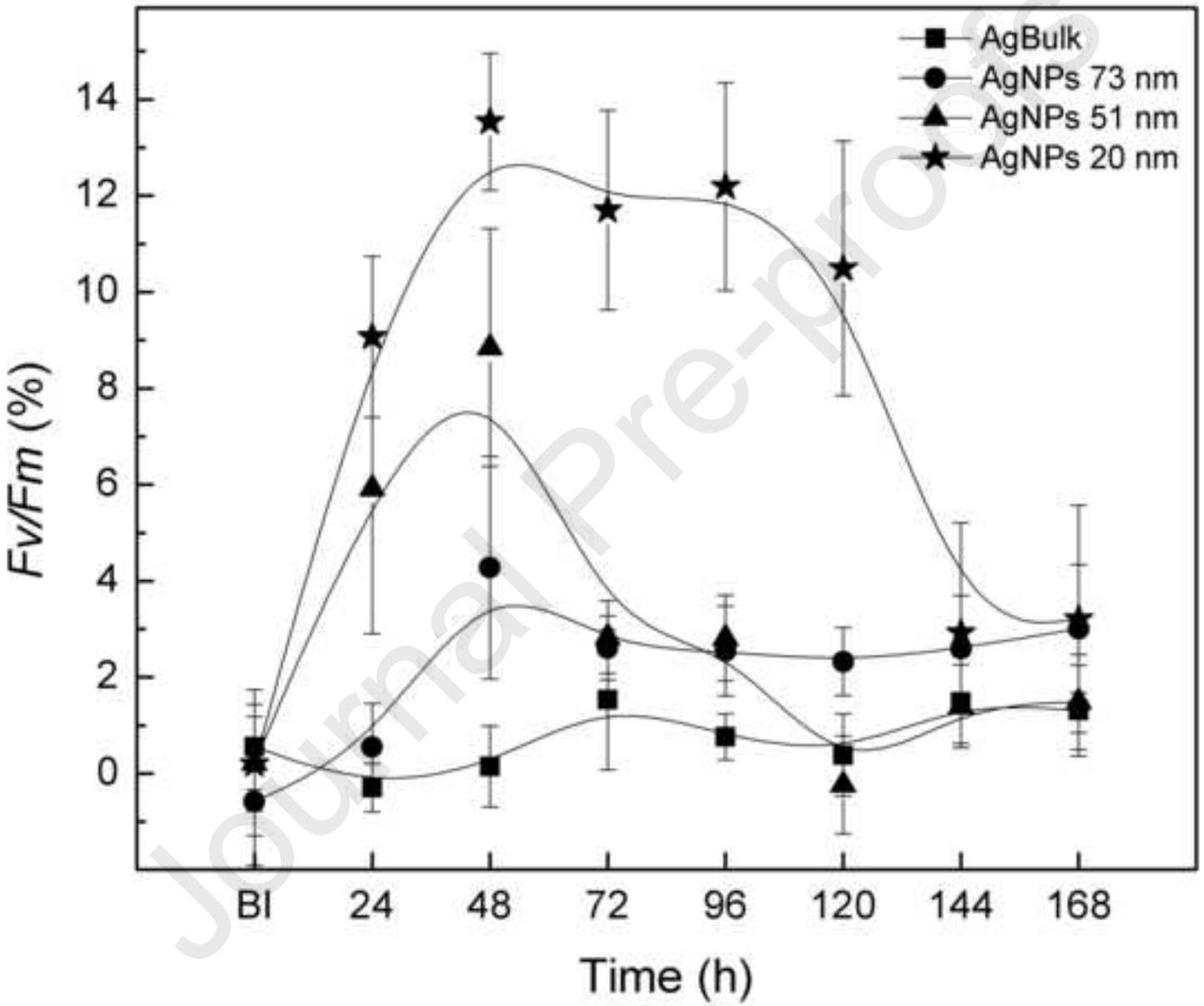

Figure 5

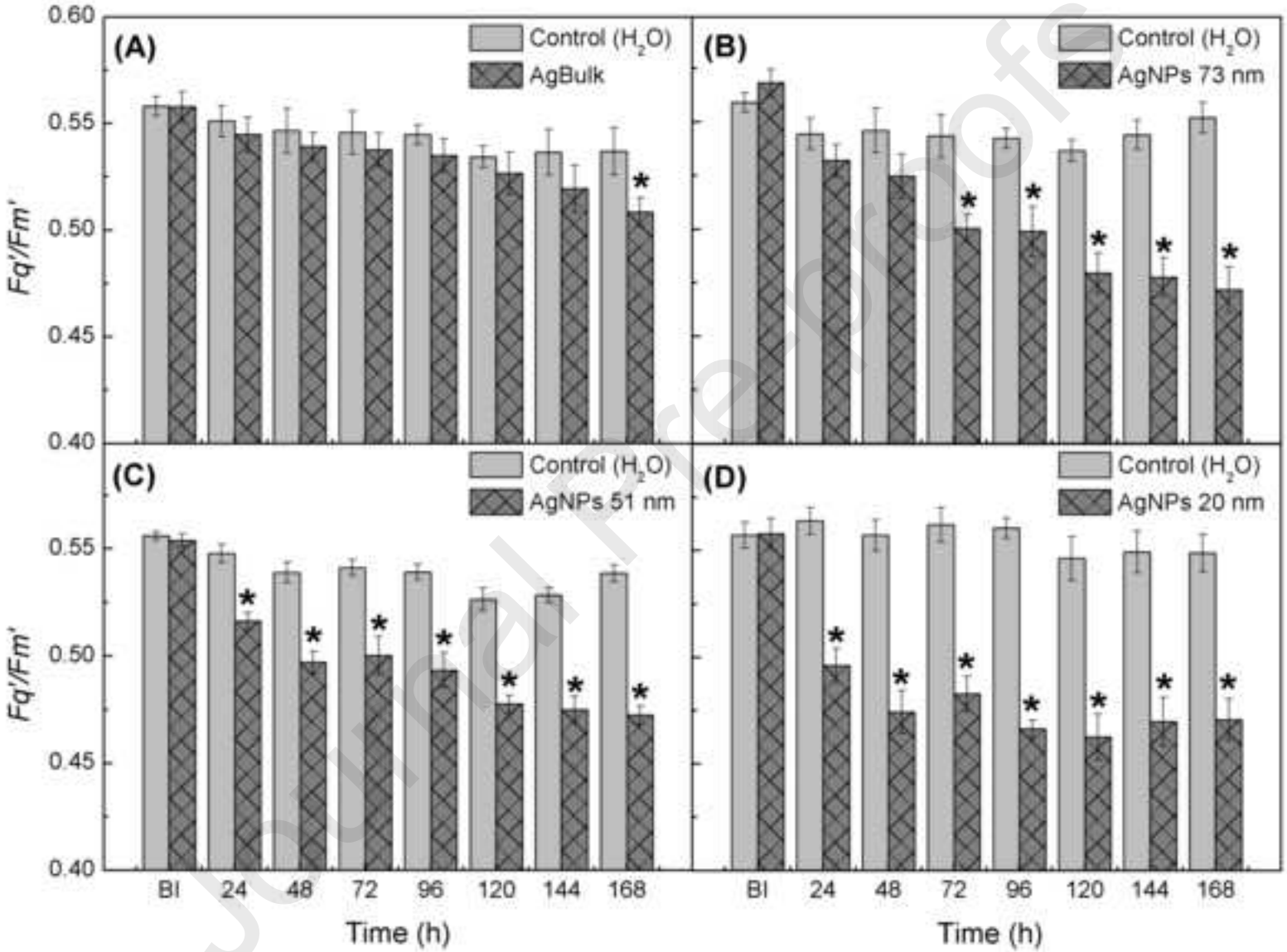

Figure 6

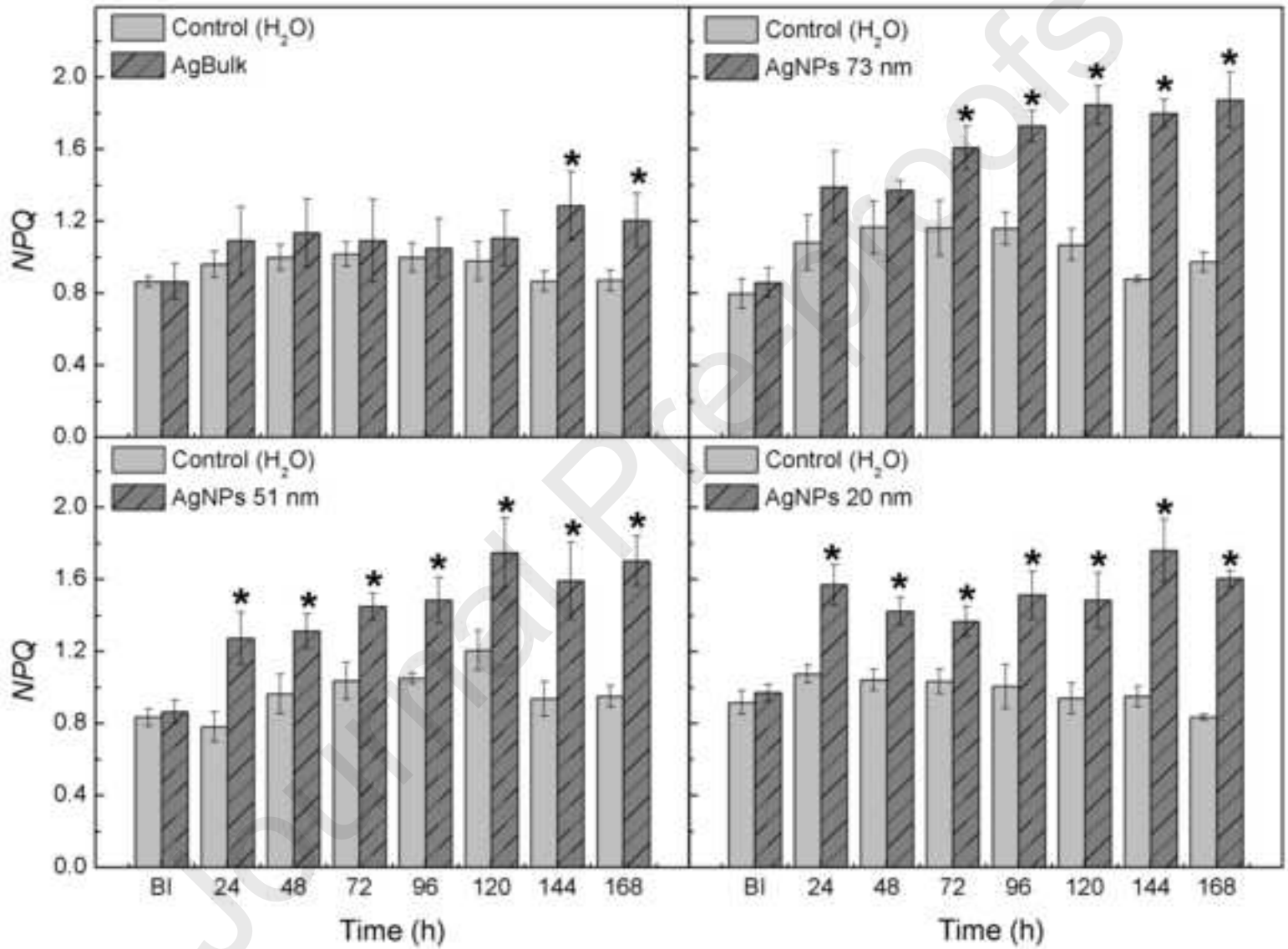

Figure 7

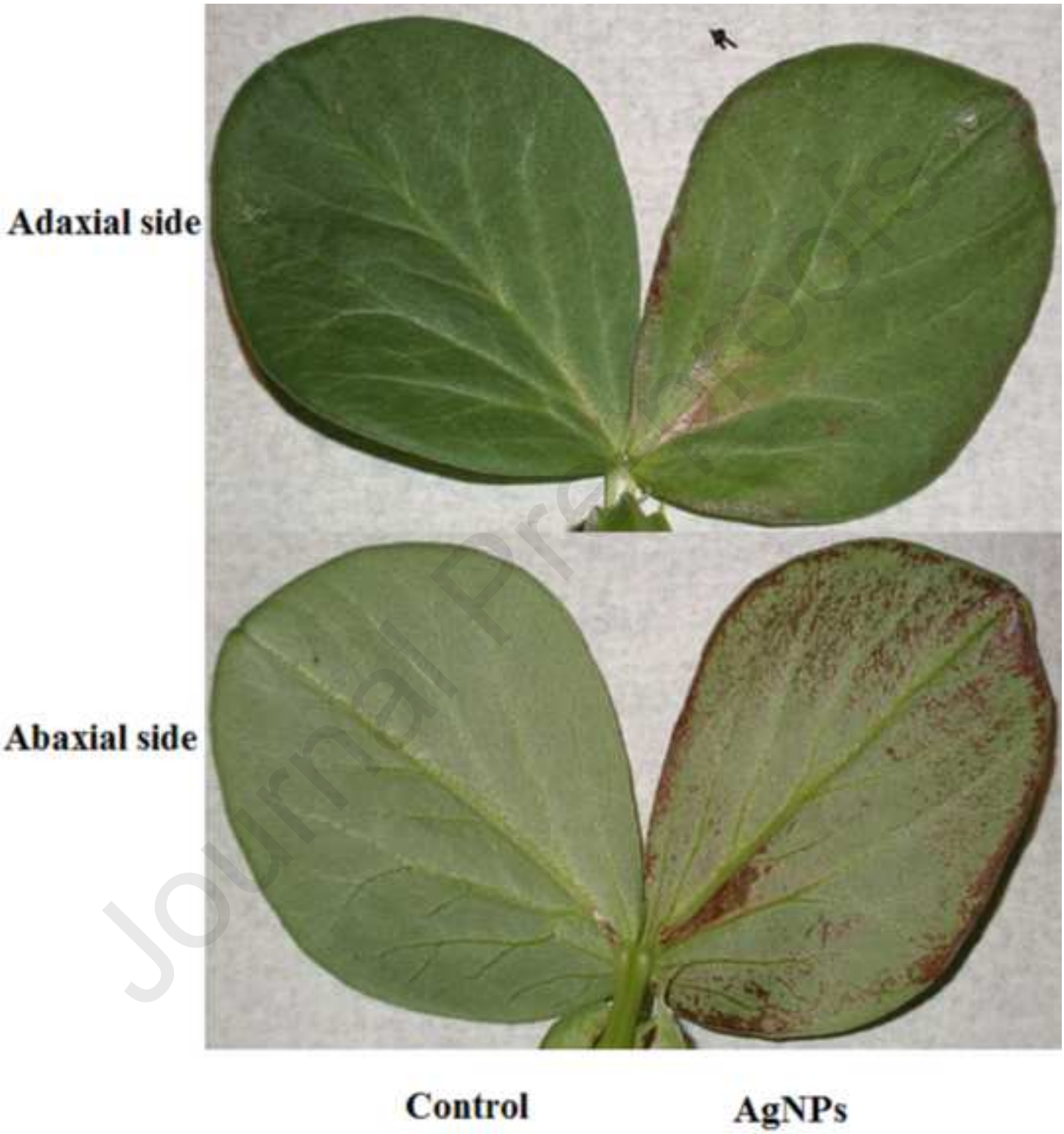

Figure 8

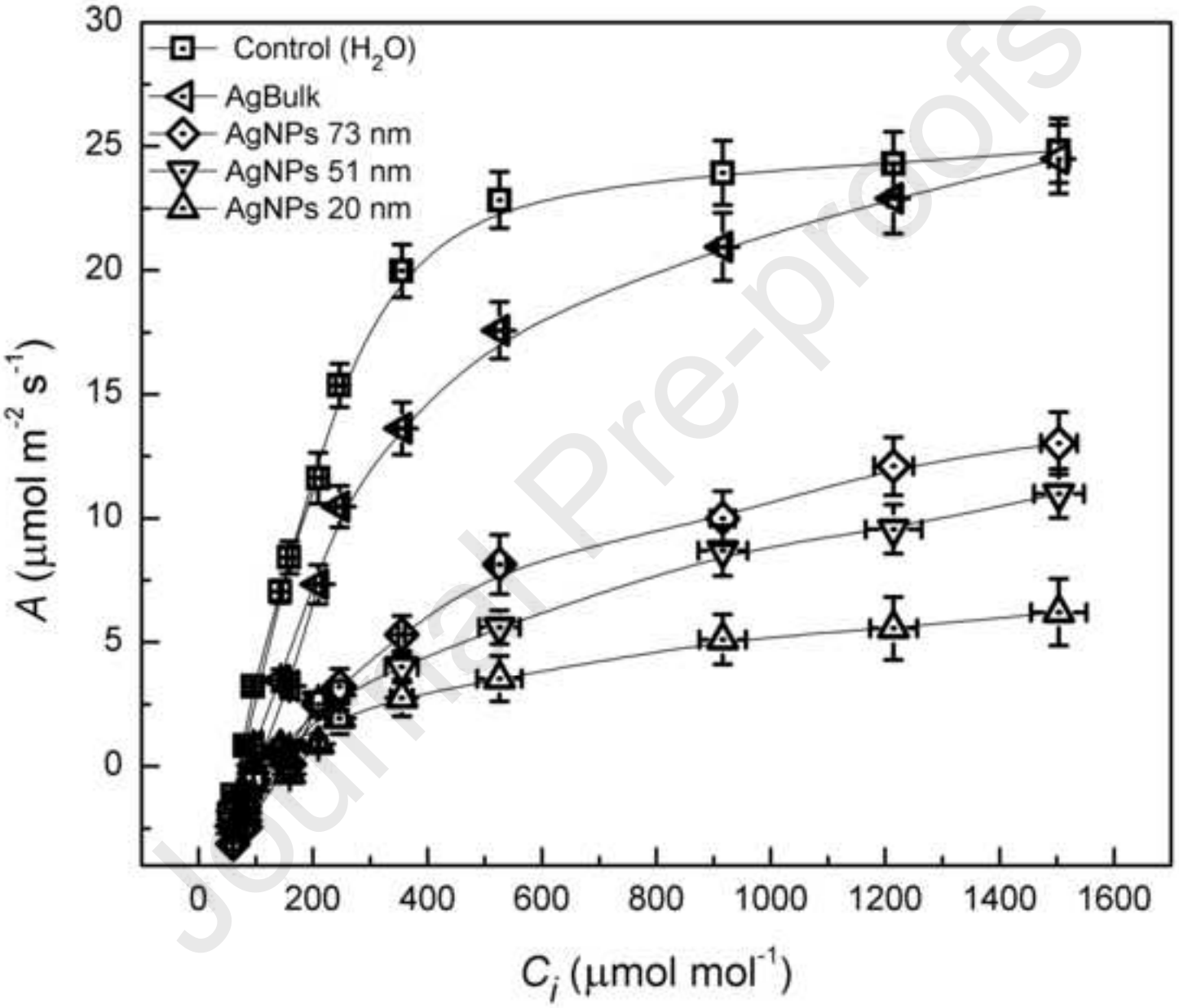

Figure 9

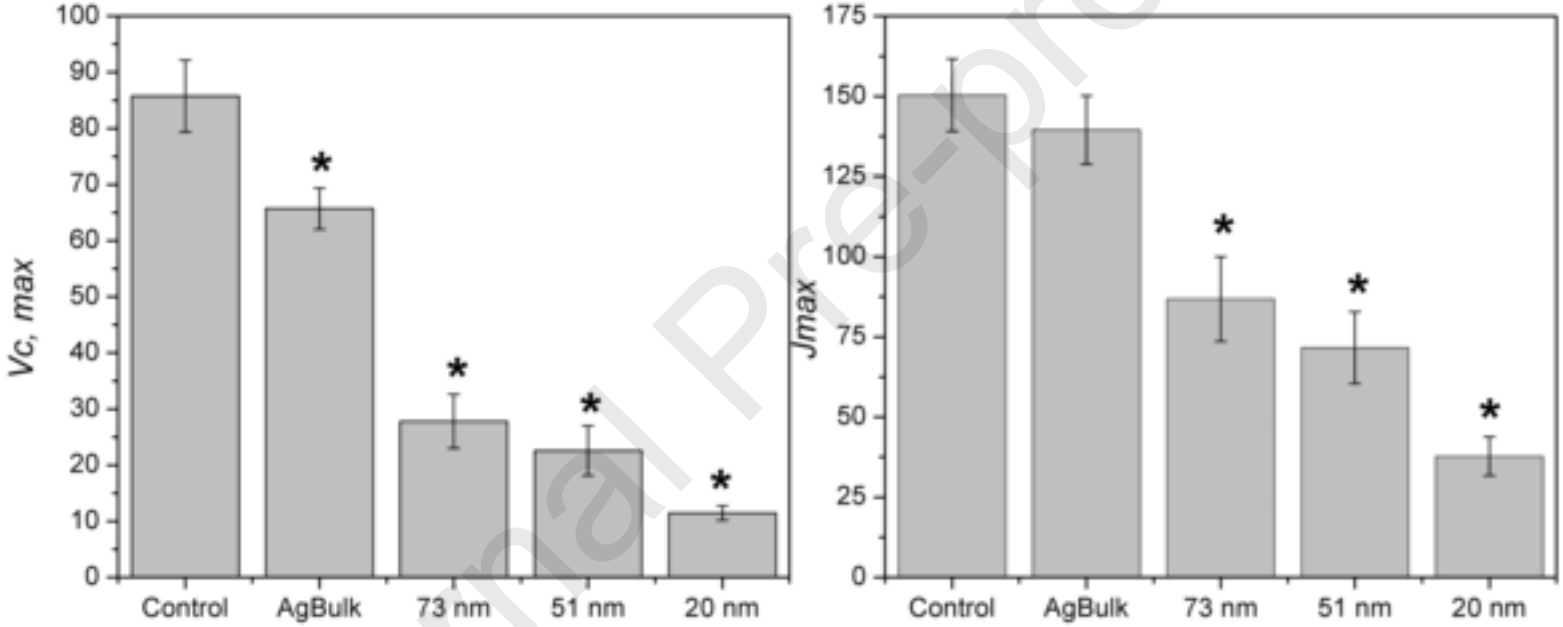

Figure 10

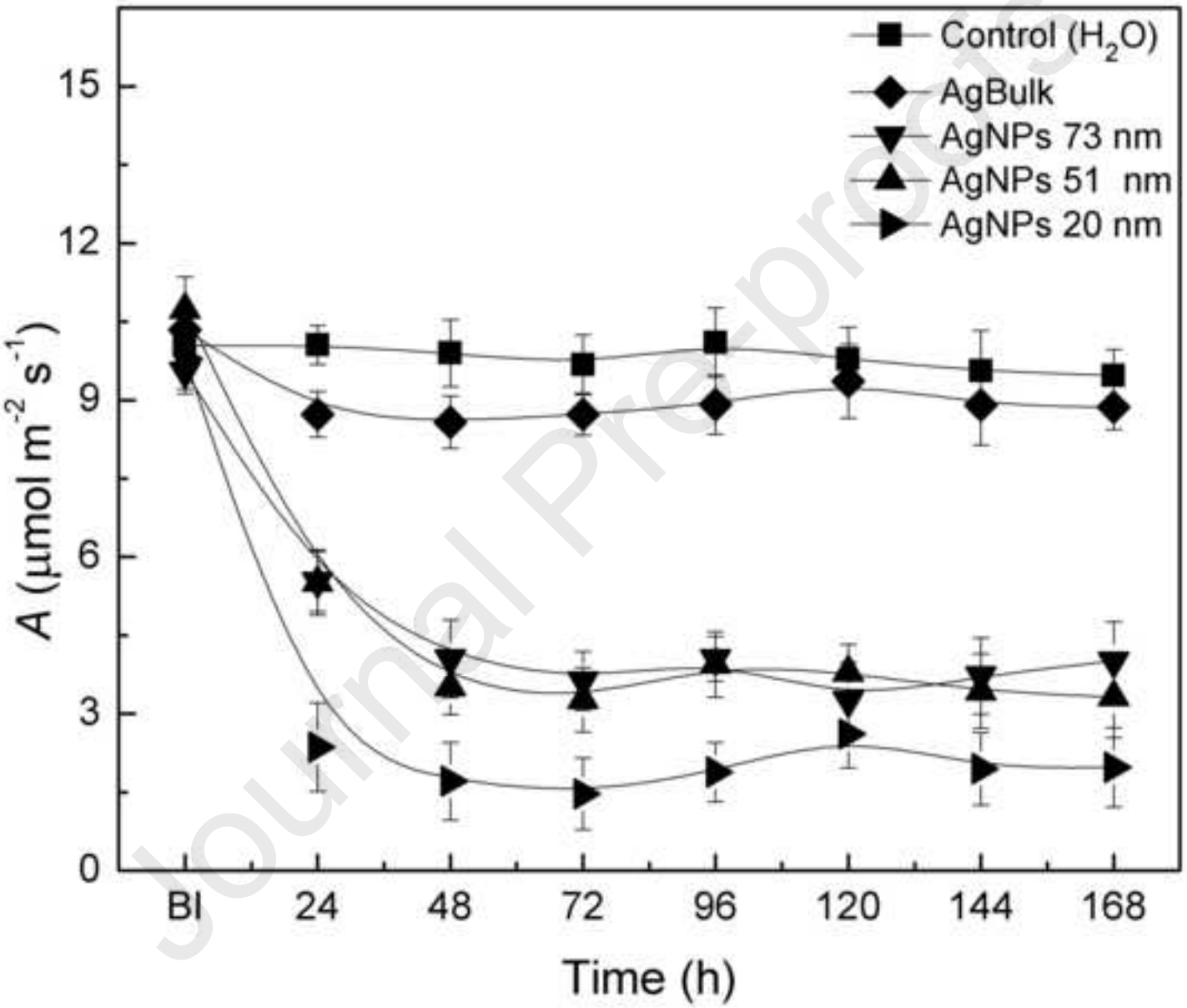

Figure 11

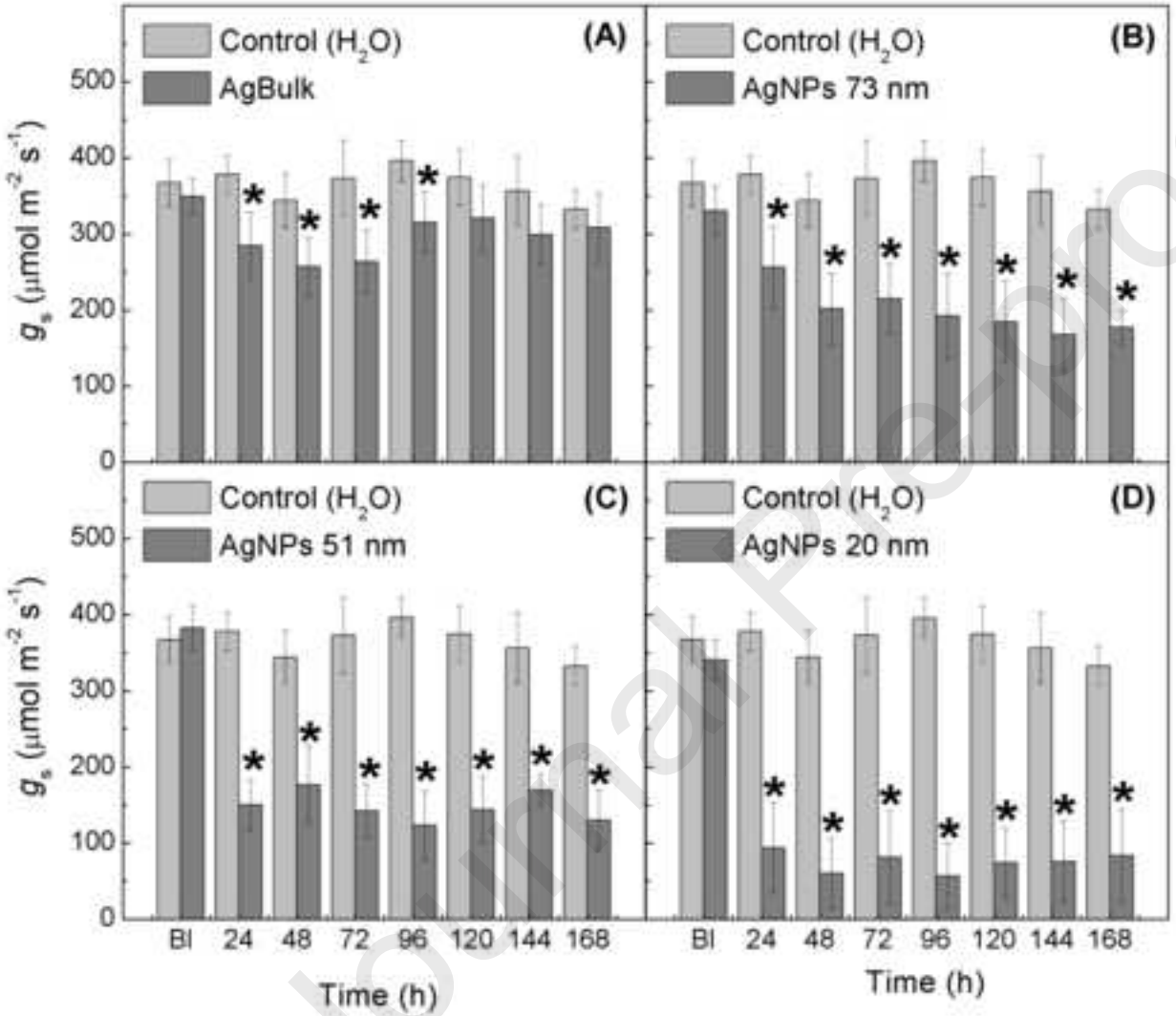

Figure 12

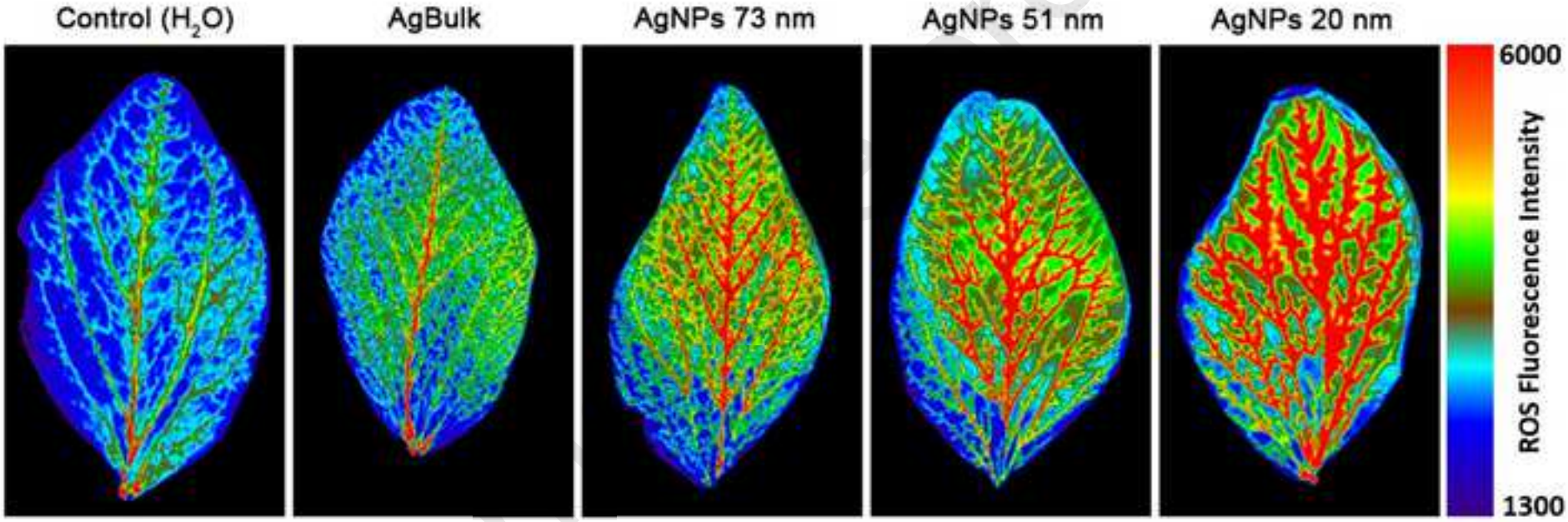

Figure 13